Advance Publication by J-STAGE
Published online 23 September 2017
KONA Powder and Particle Journal /Doi:10.14356/kona.2018014 Original Research Paper

Effect of Particle Size and Cohesion on Powder Yielding and Flow †

Hao Shi [1]*, Rahul Mohanty [2,4], Somik Chakravarty [3], Ramon Cabiscol [2], Martin Morgeneyer [3], Harald Zetzener [2], Jin Y. Ooi [4], Arno Kwade [2], Stefan Luding [1] and Vanessa Magnanimo [1]

[1] *Multi-Scale Mechanics (MSM), Faculty of Engineering Technology (ET), MESA+, University of Twente, The Netherlands*
[2] *Institute for Particle Technology (iPAT), TU Braunschweig, Germany*
[3] *Laboratoire Transformations Intégrées de la Matière Renouvelable (TIMR), Université de Technologie de Compiègne (UTC) Sorbonne Universités, France*
[4] *Institute of Infrastructure and Environment, School of Engineering, University of Edinburgh, UK*

Abstract

The bulk properties of powders depend on material characteristics and size of the primary particles. During storage and transportation processes in the powder processing industry, the material undergoes various modes of deformation and stress conditions, e.g., due to compression or shear. In many applications, it is important to know when powders are yielding, i.e. when they start to flow under shear; in other cases it is necessary to know how much stress is needed to keep them flowing. The measurement of powder yield and flow properties is still a challenge and will be addressed in this study.

In the framework of the collaborative project T-MAPPP, a large set of shear experiments using different shear devices, namely the Jenike shear tester, the ELE direct shear tester, the Schulze ring shear tester and the FT4 powder rheometer, have been carried out on eight chemically-identical limestone powders of different particle sizes in a wide range of confining stresses. These experiments serve two goals: i) to test the reproducibility/consistency among different shear devices and testing protocols; ii) to relate the bulk behaviour to microscopic particle properties, focusing on the effect of particle size and thus inter-particle cohesion.

The experiments show high repeatability for all shear devices, though some of them show more fluctuations than others. All devices provide consistent results, where the FT4 powder rheometer gives lower yield/steady state stress values, due to a different pre-shearing protocol. As expected, the bulk cohesion decreases with increasing particle size (up to 150 µm), due to the decrease of inter-particle cohesion. The bulk friction, characterized in different ways, is following a similar decreasing trend, whereas the bulk density increases with particle size in this range. Interestingly, for samples with particle sizes larger than 150 µm, the bulk cohesion increases slightly, while the bulk friction increases considerably—presumably due to particle interlocking effects—up to magnitudes comparable to those of the finest powders. Furthermore, removing the fines from the coarse powder samples reduces the bulk cohesion and bulk density, but has a negligible effect on the bulk friction.

In addition to providing useful insights into the role of microscopically attractive, van der Waals, gravitational and/or compressive forces for the macroscopic bulk powder flow behaviour, the experimental data provide a robust database of cohesive and frictional fine powders for industrially relevant designs such as silos, as well as for calibration and validation of models and computer simulations.

Keywords: cohesive powders, shear testers, yield locus, bulk friction, bulk cohesion, particle size effect, T-MAPPP, database

1. Introduction

Granular materials are omnipresent in our daily life and widely used in various industries such as food, pharmaceutical, agriculture and mining. Interesting granular phenomena like yielding and jamming (Liu and Nagel, 1998; Bi et al., 2011; Luding, 2016; Kumar and Luding, 2016), dilatancy (Cates et al., 2005; Van Hecke, 2009; Yang et al., 2015), shear-band localization (Alshibi and Sture, 2000; Singh et al., 2014), history-dependence (Thakur et al., 2014), and anisotropy (Radjai et al., 1996; Majmudar and Behringer, 2005) have attracted significant scientific interest over the past decades (Savage and Hutter, 1989; Cundall, 1989; Radjai et al., 1999; Wolf et al., 2000;

† Received 10 May 2017; Accepted 27 June 2017
J-STAGE Advance published online 23 September 2017
[1] P.O. Box 217, 7500 AE Enschede, The Netherlands
[2] Volkmaroder Str. 4-5, 38104 Braunschweig, Germany
[3] Rue Roger Couttolenc, CS 60319, 60203 Compiègne Cedex, France
[4] Edinburgh EH9 3JY, Scotland, UK
* Corresponding author: Hao Shi
E-mail: h.shi-1@utwente.nl
TEL: +31(0)53-489-6445

Copyright © 2017 The Authors. Published by Hosokawa Powder Technology Foundation. This is an open access article under the CC BY license (http://creativecommons.org/licenses/by/4.0/).

GDR-MiDi, 2004; Tomas, 2005; Alonso-Marroquin and Herrmann, 2004; Luding 2005a, b, 2008). Various laboratory element tests can be performed to study the bulk behaviour of granular materials (Schwedes, 2003). Element tests are also a valuable tool to understand the influence of particle properties, e.g. density, size-distribution and shape, on the macroscopic bulk response. Moreover, such element tests are commonly used for the industrial designs of silos (Jenike, 1967; Schwedes and Schulze, 1990; Schulze, 2003a).

Element tests are (ideally homogeneous) macroscopic tests in which the force (stress) and/or displacement (strain) path are controlled. The most widely performed element test in both industry and academia is the shear test, where a granular sample is sheared until failure is reached and the material starts to flow. Shear testers are usually classified into two groups: direct and indirect methods (Schwedes, 2003; Schwedes and Schulze, 1990). In direct shear testers, the shear zone is pre-defined by the device design, and the shear failure is forced in a specific physical location. On the contrary, in the indirect devices, the shear zone develops according to the applied state of stress. The most common indirect devices are the uniaxial compression tester (Russell et al., 2014; Thakur et al., 2014; Imole et al., 2016) and bi-axial shear box (Morgeneyer et al., 2003; Morgeneyer and Schwedes, 2003; Feise and Schwedes, 1995). Direct devices can be further categorised into two sub-groups: translational and rotational. Typical translational shear testers include the direct shear tester (Casagrande, 1936; Schwedes, 1979; Shibuya et al., 1997) and the Jenike shear tester (Jenike, 1964), while torsional or rotational shear testers include the FT4 powder rheometer (Freeman, 2007), the Schulze ring shear tester (Schulze, 1994) and the Brookfield powder flow tester (Berry et al., 2015). Detailed reviews of testers have been presented by several authors (Schwedes, 2003; Tsunakawa and Aoki, 1982; Schulze, 2008), and more (non-commercial) shear testers with higher complexity can be found in literature (Harder and Schwedes, 1985; Janssen and Zetzener, 2003; Bardet, 1997).

Quality and reproducibility of results are key aspects for proper material characterization. Although shear testing technologies have been developed and studied extensively, significant scatter in measurements is still common when testing powder flowability using different devices in different labs/environments (Freeman, 2007; Schulze, 1994; Berry et al., 2015; Schulze, 2001; Kamath et al., 1993; Kamath et al., 1994). Previous studies have been focusing on this problem by performing round-robin experimental studies on the Jenike tester (Akers, 1992), the Schulze ring shear tester (Schulze, 2001) and the Brookfield powder flow tester (Berry et al., 2015) as well as comparing different devices (Koynov et al., 2015). The earliest round-robin study (Akers, 1992) resulted in a certified material (CRM-116 limestone powder) and a common standard experimental testing procedure for determining the yield locus. Schulze (Schulze, 2011) has collected 60 yield loci obtained using the small Schulze shear tester RST-XS (21 labs) and 19 yield loci using the large Schulze shear tester RST-01 (10 labs) on one limestone powder (CRM-116). Results have been compared among them as well as with the results from reference Jenike tester. While results from RST-01 and RST-XS are in good agreement, a considerable deviation (up to 20 %) was observed when comparing results from the Schulze ring shear tester to the Jenike shear tester. Similar outputs are found by other researchers (Berry et al., 2015; Koynov et al., 2015; Salehi et al., 2017), where yield loci from the Brookfield powder flow tester, the Schulze ring shear tester, the FT4 powder rheometer and the Jenike shear tester are compared. The Brookfield powder flow tester and the FT4 powder rheometer show systematically lower shear responses in comparison to the other two shear testers.

Other studies have compared different industrially relevant powders but only in a single device (Teunou et al., 1999; Fitzpatrick et al., 2004). Moreover, these comparative studies have been limited to relatively low stresses. A deeper understanding of the flow behaviour of powders in several shear devices over a wide stress range is still missing.

Our collaborative network, EU/ITN T-MAPPP (www.t-mappp.eu), offers the unique possibility to shed light on the complex topic of powder yielding and flow, extending beyond the boundaries of previous projects. The network involves 16 partners in both academia and industry across Europe. The present study has multiple goals. Firstly, we want to investigate the consistency and repeatability of yield loci measurements between commonly used shear testers. This can provide a robust platform to establish the reliability of the testing methodology and procedures. Secondly, we aim to study the influence of cohesion on powder flowability by testing powders that have same chemical composition but different particle size, leading to different degrees of bulk cohesion. Finally, once the agreement between the shear devices is established, measurements can be combined to characterise the powders over a wider stress range, which is not achievable with a single device. To achieve this goal, a systematic study has been carried out by testing 8 powders (Eskal limestone with median particle diameter from 2.2 to 938 μm) in 5 shear testers (the Jenike Shear Tester, the Direct Shear Tester, the Schulze Ring Shear Tester with two shear cell sizes, and the FT4 Powder Rheometer) at 4 partner locations by different operators. Limestone powder has been chosen due to its negligible sensitivity towards humidity and temperature changes.

The work is structured as follows: In section 2, we provide information on the limestone samples/materials, in

section 3 the description of the experimental devices and in section 4 the test procedures. Sections 5 and 6 are devoted to the discussion of experimental results with focus on shear devices and materials, respectively, while conclusions and outlook are presented in section 7.

2. Material description and characterization

In this section, a brief description of the limestone samples along with their material properties is provided. Eight size grades with the same chemical composition, i.e. Eskal limestone (calcium carbonate), are used, with median particle sizes that almost span three orders of magnitude from µm to mm.

The Eskal series (KSL Staubtechnik GmbH, Germany) is extensively used in many fields including construction and automotive industries. Eskal is also used as a reference powder for standard testing and calibration of equipment in powder technology, for instance, shear testers (Feise, 1998; Zetzener and Schwedes, 2002) and optical sizing systems due to the favourable physical properties: high roundness, low porosity and an almost negligible sensitivity towards humidity and temperature changes, which allows to avoid sample pretreatment.

Table 1 summarizes the physical properties of the Eskal samples. Median particle size d_{50} ranges from 2.22 µm (cohesive, sticky primary particles that form clumps) to 938 µm (free-flowing primary particles). In this study, all powders are named with their original commercial name (e.g. Eskal150, Eskal300), except for Eskal K0.1–0.5 and K0.5–0.8 (original product names are Eskal Körnung 0.1–0.5 and Körnung 0.5–0.8), which for sake of brevity, is referred to as "K". The particle size distributions were determined by laser diffraction (HELOS + RODOS, Sympatec GmbH) with the dry dispersion unit. The span of the particle size distribution decreases with increasing particle size from 1.52 to 0.7, whereas the initial bulk density (bulk density measured directly after filling) increases from 540 to 1400 kg/m^3. Primary particle density ρ_p is measured using a helium pycnometer at 0.9 % moisture content and is found to be independent of size. Particle roundness, which is the ratio of the perimeter of the equivalent circle to the real perimeter of the projected primary particle, was measured with the Sympatec-QICPIC imaging system. The working principle of this technique consists of a high-speed image analysis sensor capable of capturing 500 frames per second with low exposure time below 1 ns; this set-up allows to capture and measure with a high detail size and shape information of an extremely large number of particles in the size range of 1 µm to 30 mm (Witt et al., 2006). Values are the average over approximately the range between 20000 and 8000000 particles, depending on the median size of primary particles in the powders. The median particle size, d_{50}, is used in the following as reference to the different Eskal samples.

Figs. 1 and **2** show the scanning electron microscopy images of Eskal30 and Eskal K0.1–0.5, in two different length scales. The topography of the surfaces are created using secondary electron imaging (SEI) method. In **Fig. 1**, we see that all the Eskal30 primary particles have similar shapes (left) and rough surfaces (right). But for Eskal K0.1–0.5, in **Fig. 2**, we observe more fines between the coarse particles (left) as well as on the surface (right). The other Eskal samples have mostly similar shapes (difference

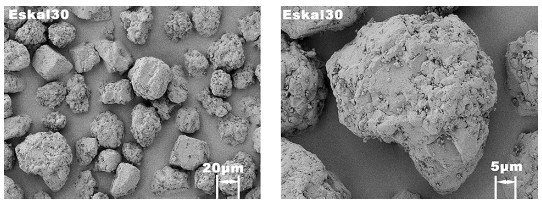

Fig. 1 SEM topography images of Eskal30 (d_{50} = 30 µm) in two different length scales as shown in the scale bars.

Table 1 Material parameters of the experimental samples. The initial bulk density represents bulk density from raw materials. Here, K0.1–0.5 means Körnung 0.1–0.5, which follows the commercial product naming. The initial bulk density values are provided by the manufacturer.

Property (Eskal)		Unit	300	500	15	30	80	150	K0.1–0.5	K0.5–0.8
Particle size	d_{10}	µm	0.78	1.64	12	21	39	97	4.5	738
	d_{50}	µm	2.22	4.42	19	30	71	138	223	938
	d_{90}	µm	4.15	8.25	28	43	106	194	292	1148
Span	$(d_{90}-d_{10})/d_{50}$	[–]	1.52	1.50	0.84	0.73	0.94	0.70	1.29	0.44
Particle density	ρ_p	kg/m^3	2737	2737	2737	2737	2737	2737	2737	2737
Moisture content	w	%	0.9	0.9	0.9	0.9	0.9	0.9	0.9	0.9
Roundness	Ψ	[–]	0.75	0.55	0.48	0.66	0.84	0.88	0.74	0.85
Initial bulk density	ρ_0	kg/m^3	540	730	1110	1230	1330	1370	1400	1276

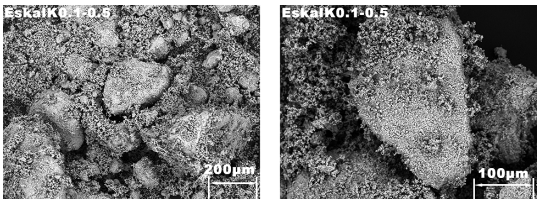

Fig. 2 SEM topography images of Eskal K0.1–0.5 (d_{50} = 223 μm) in two different length scales as shown in the scale bars.

in the range of 20 %, considering the mean values of roundness) irrespective of median particle size of the samples.

3. Experimental set-up

Many testers have been devised for measuring the yielding and flow properties of bulk solids in the last 70 years, ranging from the Jenike Shear Tester to the semi-automated or fully automated testers that are being developed in the present days (Carr and Walker, 1968). Here we present a comparison between measurements in five direct shear devices, specifically the two "translational" devices, namely the ELE direct shear tester and the Jenike shear cell, and three "rotational" devices (The Schulze ring shear testers and the FT4 powder rheometer).

A detailed comparison between the main features of all testers is shown in **Table 2** and a comparison of results from all these testers is presented in section 5. Two main characteristics of these devices are the degree of automation and the normal stress regime. The Schulze ring shear tester and the FT4 powder rheometer are in most of the operational stages completely automated, which strongly reduces the operator influences. The ELE direct shear tester can reach the highest normal stress among all the devices we investigated.

3.1 Jenike shear tester

The Jenike tester is a direct translational shear tester, developed in the 1960s (Jenike, 1964) and it is recognized as one of the industrial standards for designing reliable bulk solids handling equipment such as storage bins, silos and hoppers. The tester consists of a shear cell (D = 93 mm) which includes a closed-bottom hollow base fitted to a fixed bearing plate. A shear ring capable of moving horizontally is placed over the base with a top lid, used to close the cell, see **Fig. 3(a)**. The shear cell is filled with

Table 2 Specification comparison of the Schulze ring shear tester (RST-1), ELE direct shear tester (DST), FT4 powder rheometer (FT4) and Jenike shear cell (Jenike). The actual shear velocities used are indicated in parentheses, stars refer to the default value from control softwares.

Property	Jenike	DST	RST-01	RST-XS	FT4
Cell volume (cm^3)	189	126	204	31.4	86.4
Cell geometry	cylinder	box	ring	ring	cylinder
Wall material	aluminium	stainless steel	aluminium	aluminium	borosilicate glass
Diameter (D) or Length (L) (cm)	9.3	6	6 (inner) 12 (outer)	3.2 (inner) 6.4 (outer)	5
Height (H) (cm)	2.8	3.5	2.4	1.3	4.4
Aspect ratio H/D or H/L	0.30	0.58	0.27	0.27	0.88
Shear displacement limit (mm)	8	10	unlimited	unlimited	unlimited
Test control	Manual	Manual	Computer	Computer	Computer
Sample weighing	offline	offline	offline	offline	on-board
Compression device	top lid	top lid	top ring	top ring	vented piston
Driving velocity	1–3 (2) (mm/min)	0.001–2 (2) (mm/min)	0.0038–22.9 (*) (°/min)	0.0038–22.9 (*) (°/min)	6–18 (6) (°/min)
Max. normal stress (kPa)	10–30	2778	50	20	22
Sample conditioning before pre-shear	pluviation (manual)	pluviation (manual)	pluviation (manual)	pluviation (manual)	rotated blade (automatic)
Yield locus test duration	2 hours	2 hours	20 mins	20 mins	30 mins
Stress measure direction	horizontal	horizontal and vertical	rotational and vertical	rotational and vertical	rotational

the test sample, which rests within the base and the shear ring, as shown in **Fig. 3(b)**. A normal force is applied to the shear lid by loading weight on a hanger. A shear force is then applied using a bracket and a pin on the shear ring. The bulk solid undergoes shear deformation due to the simultaneous displacement of the upper ring and the lid against the stationary bottom ring. The stem is moved by a motor at a constant speed of around 1–3 mm/minute and the shear force is measured by a force transducer and is recorded on a computer.

For conducting a shear test, a sample of powder is uniformly filled into the shear cell using a spatula and/or a sieve. The sample is initially pre-consolidated by twisting a special lid covering the powder bed under a certain normal load. Then the lid and the filling ring are replaced with a shear lid and the pre-consolidated sample is pre-sheared until a steady state flow is reached, which is defined as a state of constant shear force and bulk density for a given normal stress. After retracting the shear stem and reducing the normal load, the shearing process is re-initiated under a reduced normal load until a maximum shear stress is recorded. This peak value represents a single point on the yield locus. The pre-shear and shear process is repeated for lower normal loads in order to get the complete yield locus. A more detailed description of the standard testing procedure is reported in the ASTM standard D-6128 (ASTM-D6128, 2006). The laborious work of filling and sample conditioning as well as a potential influence of the operator are the major drawbacks of this technique.

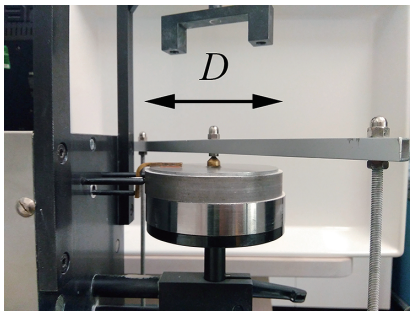

(a)

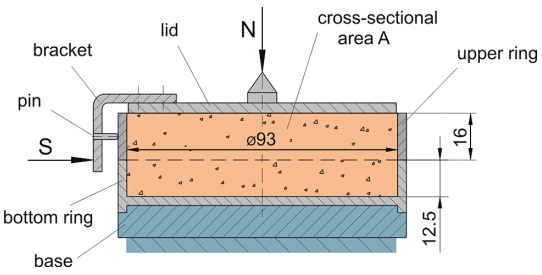

(b)

Fig. 3 **(a)** Jenike direct shear tester and **(b)** the schematic representation of the Jenike shear cell. For technical details see **Table 2**. **Fig. 3(b)**, reprinted with permission from author (Schulze, 2002). Copyright: (2002) Dietmar Schulze.

3.2 ELE direct shear tester (DST)

The second direct shear tester (ELE International, United Kingdom), is illustrated in **Fig. 4(a)**. It operates with specimens with a square cross-section of 60 mm × 60 mm and a height of 30 mm. The apparatus is enclosed in a robustly constructed case. It is designed for and can reach shear stress up to 1250 kPa and normal stress up to 2778 kPa. The speed range is between 0.0001 to 2 mm/min. The ELE direct shear tester is designed for much higher load in soil testing, employs a simple shear principle as the Jenike shear cell, has a larger shear displacement range (up to 12 mm in horizontal direction) and the possibility of reverse box movement.

The shear test sequence starts with the filling of the shear box by dry pluviation of the powder into the box until a height of approximately 40 mm is reached; then

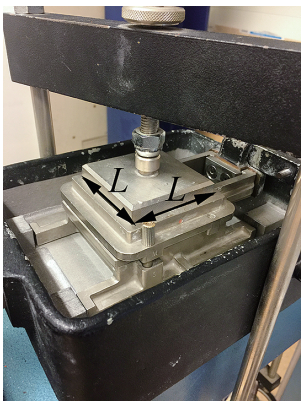

(a)

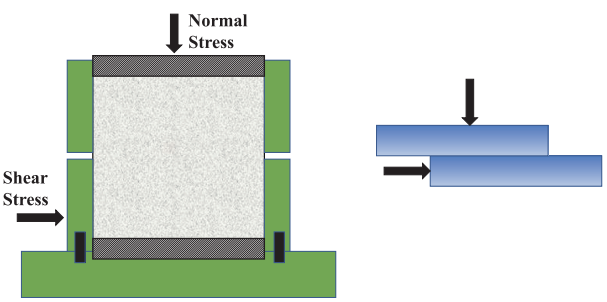

(b)

Fig. 4 **(a)** The ELE direct shear tester and **(b)** the schematic representation of the ELE direct shear cell set-up. For technical details see **Table 2**.

the top excess powder is removed by a scraper to ensure that the top surface of the sample is flat. Finally the top lid is mounted and the powder sticking to the sides of the box is removed carefully using a small paint brush. In addition to the typical direct shear testers as listed in Sec. 3.1, the main drawback for this tester is the possible ejection of powder through the inter-quadrate opening. In order to compare results in DST with other devices properly, shear tests in this study are performed following the same ASTM standard D-6128 (ASTM-D6128, 2006) as in Jenike shear tester. For the steady state test, in analogy to the normal wall friction procedure, the sample is first sheared to steady state at the highest normal load chosen. Then step by step the normal load is decreased and shear is continued until steady state is reached.

3.3 Schulze ring shear tester—RST-01 and RST-XS

Among the shear devices for powder characterization, the Schulze rotational ring shear tester (1994) is one of the most widely used testers. The Schulze ring shear tester (RST-01) operates connected to a personal computer running a control software that allows the user to obtain, among other things, yield loci and wall yield loci. A smaller version of the ring shear tester with exactly the same working principle is the so-called RST-XS, developed for smaller specimen volumes (3.5 ml to 70 ml, rather than 204 ml for the RST-01). For both testers, ring-shaped (annular) bottom ring of the shear cell contains the bulk solid specimen. An annular-shaped lid is placed on top of the bulk solid specimen and it is fixed at a cross-beam (**Fig. 5**).

A normal force, F_N, is exerted on the cross-beam in the rotational axis of the shear cell and transmitted through the lid onto the specimen. Thus a normal stress is applied to the bulk solid. In order to allow small confining stress, the counterbalance force, F_A, acts in the centre of the cross-beam, created by counterweights and directed upwards, counteracting the gravity forces of the lid, the hanger and the cross-beam. Shearing of the sample is achieved by rotating the bottom ring with an angular velocity ω, whereas the lid and the cross-beam are prevented from rotation by two tie-rods connected to the cross-beam. Each of the tie-rods is fixed at a load beam, so that the forces, F_1 and F_2, acting on the tie-rods can be measured. The bottom of the shear cell and the lower side of the lid are rough in order to prevent sliding of the bulk solid on these two surfaces. Therefore, rotation of the bottom ring relative to the lid creates a shear deformation within the bulk solid. Through this shearing the bulk solid is deformed, and thus a shear stress τ develops, proportional to the forces on the tie-rods ($F_1 + F_2$). All the tests performed here follow the ASTM standard (ASTM-D6773-16, 2008).

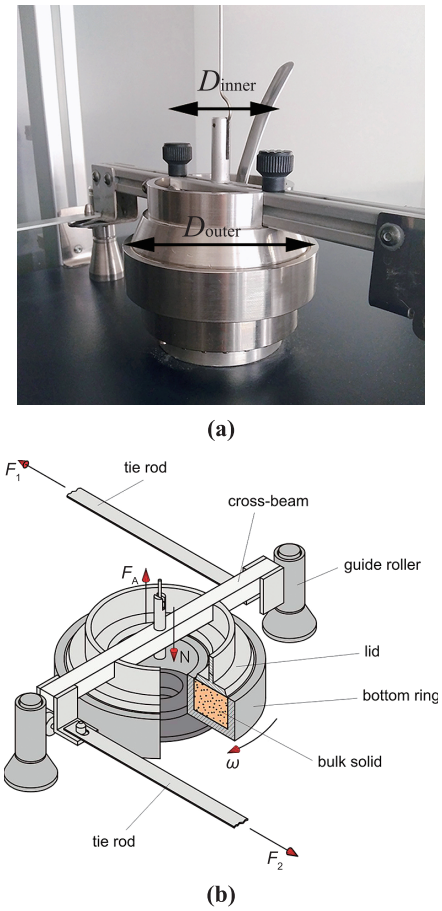

Fig. 5 **(a)** The Schulze ring shear tester RST-01 and **(b)** the working principle of the Ring shear cell set-up. The difference between RST-XS and RST-XS is the shear cell size. For technical details see **Table 2**. **Fig. 5(b)**, reprinted with permission from author (Schulz, 2003b). Copyright: (2003) Dietmar Schulze.

3.4 FT4 powder rheometer

The last experimental equipment used in this work is the FT4 Powder Rheometer (Freeman technology Ltd., UK), depicted in **Fig. 6(a)**. Standard accessories for the shear test include the 50-mm-diameter blade for sample conditioning, the vented piston for compression, the shear head for the shearing process and the 50-mm-high with 50 mm diameter borosilicate test vessel. One advantage of the commercial FT4 Powder Rheometer is the automated nature of the test procedure requiring minimal operator intervention.

The shear test sequence under the ASTM standard D7891 (ASTM-D7891-15, 2015) can be summarized as follows: the test vessel is carefully filled with the powder of interest using a spatula after obtaining the tare weight. The conditioning procedure involves the movement of the conditioning blade into the test sample to gently disturb the powder bed for a user-defined number of cycles before it is removed slowly. A cycle consists of the inward and

outward movement of the conditioning blade into the powder bed with a constant rotation movement all the time. In order to prevent the conditioning blade from touching the base of the vessel, the direction of the blade movement is reversed as soon as it is within 1 mm of the vessel base. It is believed that this creates a uniform, loosely packed test sample that can be readily reproduced (Freeman, 2007).

In this study, we perform three pre-conditioning cycles before the shear tests are carried out (pre-conditioning does not involve a confining stress like in the other 3 testers). The portion of the base insert of the test vessel are excluded from the calculation of the vessel height, leading to a maximum vessel height of 44 mm instead of 50 mm and an aspect ratio α of 0.88. Subsequent to pre-conditioning, the blade is replaced with a vented piston, which incorporates a stainless steel mesh to allow the enclosed air in the powder to escape uniformly across the surface of the powder bed. The vessel assembly is then split (and thus levelled) after the vented piston executes the compression until the pre-shear normal stress level is reached. Then the powder mass is recorded after splitting to compute the bulk density before the shear tests start. A detailed description of the vessel split-and-levelling procedure is reported by Freeman et al. (2009).

A shear test begins after changing the vented piston to the shear head as shown in **Fig. 6(b)**. The shear head moves downwards inserting the blades into the powder and induces a normal stress as the shear head bottom surface is in contact with the top of the powder. The shear head continues to move downwards until the required pre-shear normal stress is reached. At this point slow rotation of the shear head begins, inducing an increasing shear stress. As the powder bed resists the rotation of the shear head, the shear stress increases until failure, at the point a maximum shear stress is observed. As a consequence, a shear plane is formed just below the ends of the blades. The shear head is kept moving until the shear stress does not change anymore for the pre-shear step and is stopped immediately after the maximum is reached for each shear step. A constant normal stress is maintained throughout each pre-shear or shear step. Note that pre-shear in FT4 is a multi-stage process and will be discussed in the next section. All the tests performed with the FT4 powder rheometer follow ASTM standard (ASTM-D7891-15, 2015).

4. Test procedures

In this section, an overview of the testing procedures as well as all the details of the tests performed using shear devices for different limestone specimens are presented.

The diagram in **Fig. 7** illustrates the common testing procedures used for measuring the yield locus. The Schulze ring shear tester RST-01 only requires one single pre-shear cycle before the first shear point and the steady state is reached (**Fig. 7** top). And this pre-shear determination is also similar in the DST and Jenike. However, the FT4 powder rheometer involves multiple pre-shear cycles before the first shear is initiated, and it determines the steady state only when the difference between the end point shear stress values from two consecutive pre-shear cycles is within 1 % (**Fig. 7** bottom). The number of multiple pre-shear cycles in the FT4 usually varies from 4 for cohesive powders to 6 for free-flowing powders. And the influence of this difference on powder flow properties will be further elaborated in Sec. 5.3.

The main quantities referred to in this study (linearised effective yield locus, yield locus and steady state/termination locus) are explained in **Fig. 8**, where the pre-shear and shear points are the measured values as indicated in **Fig. 7**. According to these three loci, three different angles can be determined: effective angle of internal friction,

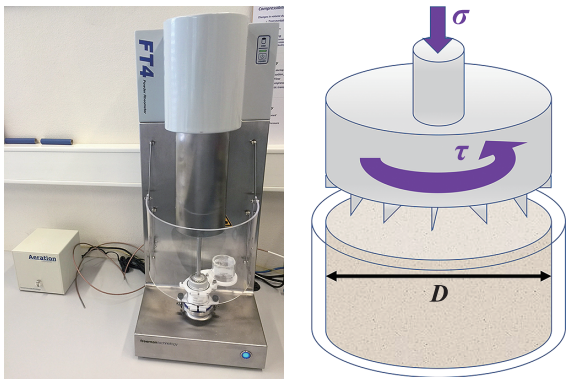

Fig. 6 **(a)** The FT4 Powder Rheometer and **(b)** the working principle of the FT4 shear cell set-up. For technical details see **Table 2**.

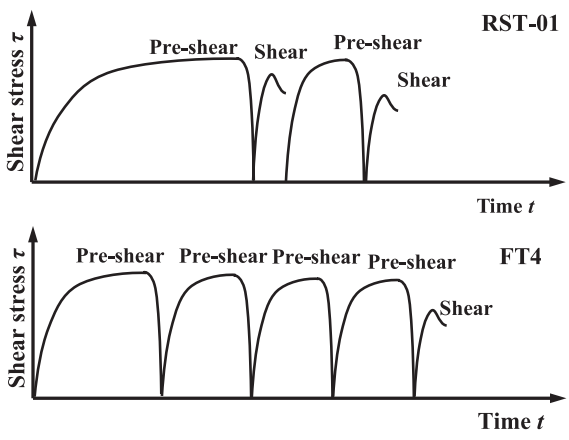

Fig. 7 Schematic drawing of typical yield locus measurement steps for RST-01 (top) and FT4 (bottom).

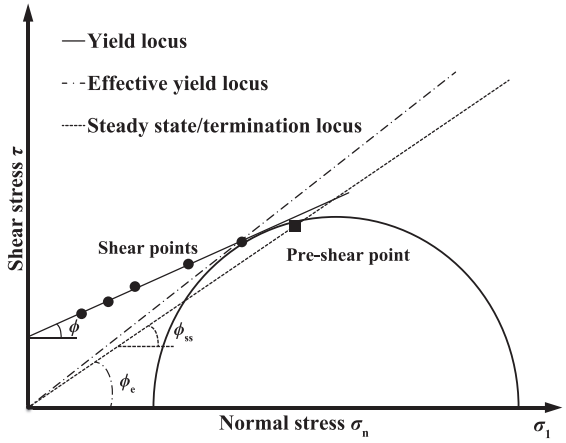

Fig. 8 Schematic drawing of effective yield locus, yield locus and steady state locus.

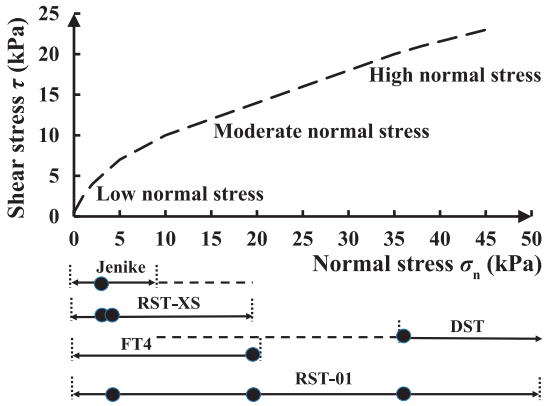

Fig. 9 Schematic drawing of typical yield locus. Black arrows at the bottom: typical normal stress ranges used for each device; dashed lines are extended normal stress limits. Black points indicate the actual normal stress levels used for different shear testers.

ϕ_e, angle of internal friction, ϕ, and steady state angle of internal friction, ϕ_{ss} as depicted in **Fig. 8** and the details are given by Schulze (2008). The intercept of yield locus for normal stress equals to zero is named as cohesive strength, and it qualitatively indicates the bulk cohesion of a given sample under a given normal stress. Note that all the quantities measured from different testers are using the same definition here.

Since all the devices investigated here have been designed for different purposes, they are adapted to test the materials in preferable normal stress ranges. In **Fig. 9**, we show schematically the range of normal stress that each device can cover with acceptable accuracy. In the same plot, we indicate the extended normal stress ranges of Jenike and DST (dashed lines). For Jeinke in higher normal stress range, the data are highly difficult to acquire and less reliable due to insufficient shear path available in shearing direction. On the other hand, low/intermediate normal stress results from DST are less accurate due to the limit of the force sensor. The actual normal stresses used for this study are also highlighted with black dots on the solid lines and summarized in **Table A1**. In **Fig. 9**, we divide the whole normal stress range into three regimes: i) low normal stress, where Jenike, RST-01/RST-XS and FT4 can be used; ii) moderate normal stress, where RST-01 and FT4 are available; iii) high normal stress that DST and RST-01 can be relied on.

The Schulze RST-01 was chosen as a reference device and used to test all 7 Eskal samples at 3 different pre-shear normal stress levels since it covers the widest stress range. A limited number of cases were tested with the other devices depending on the accuracy and material availability. However, for each pre-shear normal stress, tests on one powder have been performed using at least two devices in order to check the reproducibility of the results between the testers. Each test was repeated three times (3 fresh samples) to investigate the repeatability within a single device. Details on the pre-shear and shear normal stress levels used are given in **Table A1**. In addition, we have also performed steady state locus study using 4 powders in DST. We have chosen a pre-shear normal stress values between 1.4 and 36.1 kPa. The test details are summarized in **Table A2**.

5. Comparison of shear devices

In this section, we compare the measurement from different shear devices and a general overview of the repeatability and reproducibility of the test results is given. In order to compare the yield loci from different testers, two limestone powders were chosen as reference powders (see **Table 3**), namely cohesive Eskal300 (2.22 µm) and free flowing Eskal150 (138 µm).

Table 3 Summary of the tests performed. The numbering in the table are the number of powders tested with a certain device under a certain pre-shear stress level. For more details, see **Table A1**. Note that the values in the parentheses refer to the pre-shear normal stress values used for a specific device.

Stress in kPa Device	Low stress 5 (4.3)	Moderate stress 20	High stress 35 (36.1)
Jenike	2 (4.3)	[–]	[–]
DST	[–]	[–]	4 (36.1)
RST-01	7	8	7
RST-XS	4 (4.3)	[–]	[–]
FT4	[–]	4	[–]

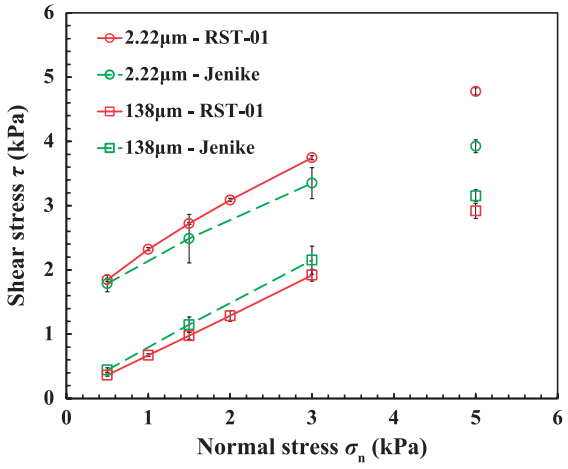

Fig. 10 Yield locus (shear stress versus normal stress) of Eskal150 (138 µm) and Eskal300 (2.22 µm) using RST-01 and Jenike. The pre-shear normal stress is kept at 5 kPa for both devices. Points with and without lines are shear and pre-shear points, respectively. Lines are guides to the eye.

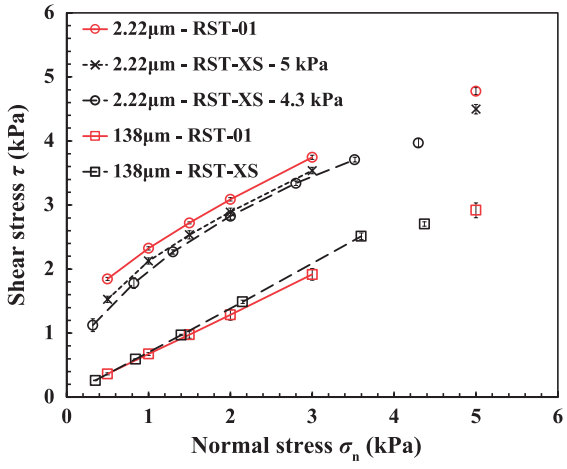

Fig. 11 Yield locus (shear stress versus normal stress) of Eskal150 (138 µm) and Eskal300 (2.22 µm) using RST-01 and RST-XS. The pre-shear normal stresses are set to 5 and 4.3 kPa for RST-01 and RST-XS, respectively (Eskal300 has one extra 5 kPa pre-shear using RST-XS). Points with and without lines are shear and pre-shear points, respectively. Lines are guides to the eye. Note that here the data for RST-01 are the same as in **Fig. 10**.

5.1 Low normal stress: Schulze ring shear tester (RST-01) vs Jenike tester

In the low normal stress regime, we first compare the RST-01 with the standard Jenike tester at pre-shear normal stress of 5 kPa. Each shear point is measured with 3 fresh samples to acquire the standard deviations. The yield loci for Eskal150 (138 µm) and 300 (2.22 µm) are shown in **Fig. 10**. Both testers show quite good repeatability with a higher standard deviation from the Jenike tester. When we look at the individual powders, the agreement between the two shear testers for Eskal150 is good, with the difference increasing slightly with increasing normal stress. The pre-shear stress values are also close within the deviation range. For the finer Eskal300, the discrepancy between the two devices becomes higher, but still within the standard deviation. A big discrepancy is observed for the pre-shear points, where the Jenike shows lower values and higher standard deviations compared to RST-01. This may be related to the manual control procedure of the Jenike shear cell. Often the pre-shear must be stopped to prevent the risk of running out the shear displacement.

5.2 Low normal stress: Schulze ring shear tester (RST-01) vs (RST-XS)

In the same low normal stress range, we have also tested the two reference powders using the smaller RST-XS, and the data are compared to RST-01 as shown in **Fig. 11**. For both devices, the repeatability is very high, with the standard deviations within the symbol size. For the free flowing Eskal150, the yield loci measured by the two devices demonstrate a very good agreement although a slightly different pre-shear normal stresses are used. For the cohesive Eskal300, data from RST-XS are consistently lower than data from RST-01. However, both devices show a non-linear behaviour with the slope (decreasing with increasing normal stress).

To further investigate RST-XS, we have tested Eskal300 in the RST-XS using the same pre-shear and shear stress levels as in RST-01, and results are also plotted in **Fig. 11**. We observe that, also in this case of same pre-shear normal stress, the RST-XS values are systematically lower than the RST-01 values (around 5 %). As the only known difference between RST-XS and RST-01 is the shear cell size, our results indicate that the powder response may be influenced by the system size in the case of cohesive material.

5.3 Moderate normal stress: Schulze ring shear tester (RST-01) vs FT4 powder rheometer

In the moderate normal stress regime, we compare the most commonly used rotational shear testers, the RST-01 and the FT4 rheometer. Both testers are automated and allow selection of a pre-shear normal stress value, σ_{pre}, which was set to 20 kPa for our comparison.

The yield loci for Eskal300 and Eskal150 are shown in **Fig. 12**. Both the RST-01 and the FT4 show good repeatability for each measurement point, with the standard deviations within the symbol size. For the free-flowing Eskal150, the yield loci measured by the two devices are in very good agreement except for the pre-shear points,

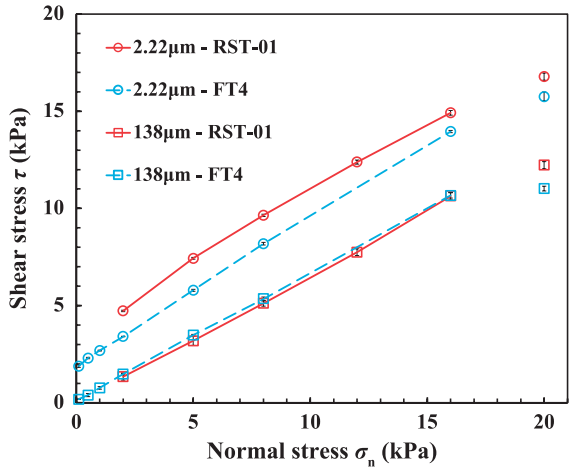

Fig. 12 Yield locus (shear stress versus normal stress) of Eskal150 (138 μm) and Eskal300 (2.22 μm) using RST-01 and FT4. The pre-shear normal stress is kept at 20 kPa for both devices. Points with and without lines are shear and pre-shear points, respectively. Lines are guides to the eye.

where the FT4 gives a much lower value than the RST-01. However, for the cohesive Eskal300, we see a pronounced difference between results obtained by the two devices (around 10–20 %), although the angle of internal friction (slope) between the two devices stays almost the same. A similar trend is observed with the other two cohesive samples: Eskal500 and Eskal15, with the values measured by FT4 systematically lower than the ones from RST-01 (data not shown here, for details see **Tables B1** and **B2**).

We associate the difference in the behaviour between the two devices to the test protocols as explained in Sec. 4. The Schulze ring shear tester, based on the ASTM standard D-6773 (ASTM-D6773-16, 2008), uses the conventional pre-shear determination criterion: the steady state shear stress plateau is determined in one pre-shear stage and the following pre-shear stages after incipient flow follows this one pre-shear state value. On the other hand, for the FT4 powder rheometer, based on the ASTM standard D7891 (ASTM-D7891-15, 2015), several pre-shear cycles are performed until the steady state reaches a constant shear stress value (within 1 % difference). This value is the assumed as pre-shear steady state and the shear stage starts. In the case of cohesive powders, the samples need 3–10 repetitions for the pre-shear to fulfil the steady state criterion in the FT4. This may lead to formation of a pre-defined shear failure plane in the sample that reduces its shearing resistance along the shear direction. We point out here that both shear devices are automated using their own test software where the test protocols are in-built and therefore impossible to change by the users. In addition, there is another significant difference between the two testers in that the Schulze ring shear tester has an annular cross-section where the shear displacement is applied fairly uniformly over the solid shearing surface; whilst the FT4 rheometer has a circular cross-section where the shearing displacement is highly non-uniform with values decreasing towards zero at the centre of the cross-section. It is thus probable that critical shearing state may not be fully achieved particularly near the central zone of the cross-section, thereby producing a smaller overall critical shear stress.

5.4 High normal stress: Schulze ring shear tester (RST-01) vs direct shear tester (DST)

In the high normal stress regime, we compare the reference Schulze ring shear tester (RST-01) with the direct shear tester (DST) as shown in **Fig. 13**. The pre-shear stress σ_{pre} is set to 35 kPa for the RST-01 and 36.1 kPa for the DST. This small difference in the pre-shear normal stress applied is due to the design limitation of DST, where one can only change the normal stress discontinuously.

As we can see clearly from the figure, the results from DST and RST-01 are in good agreement for both powders. The standard deviation of DST data is higher than the RST-01, and becomes more prominent for low stress levels as well as for the free-flowing sample Eskal150. In the case of pre-shear points, the DST shows a slightly lower value compared to the RST-01, but the difference is negligible. For the yield locus of Eskal150, data from the two devices overlap within the error bars. When we focus on Eskal300, DST underestimates the shear stress values on the yield locus with respect to the RST-01, especially for low normal stresses. We want to point out that the low stress data from DST may be less reliable that the shear

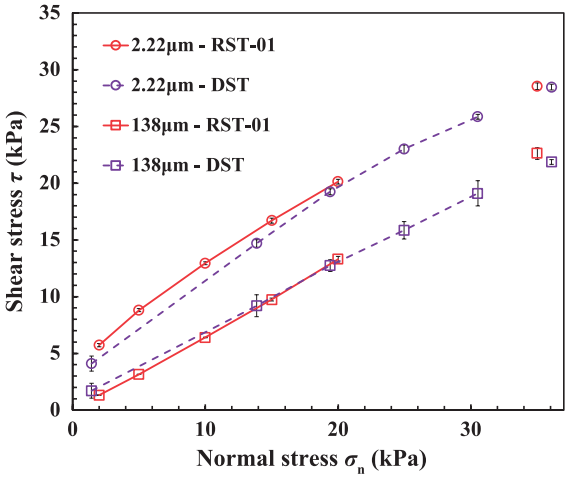

Fig. 13 Yield locus (shear stress versus normal stress) of Eskal150 (138 μm) and Eskal300 (2.22 μm) using RST-01 and DST. The pre-shear normal stresses are kept at 35 and 36.1 kPa for RST-01 and DST, respectively. Points with and without lines are shear and pre-shear points, respectively. Lines are guides to the eye.

force measurement system of DST has a lower limit value of 1 N (1 kPa).

Finally, in order to confirm the reproducibility between the two devices, we further test the steady state shear responses for Eskal K0.1–0.5 and Eskal K0.5–0.8, as shown in **Fig. 14**. Results from the two shear devices show good agreements for the tested two powders, with the data points following the two linearised yield loci within the standard deviations.

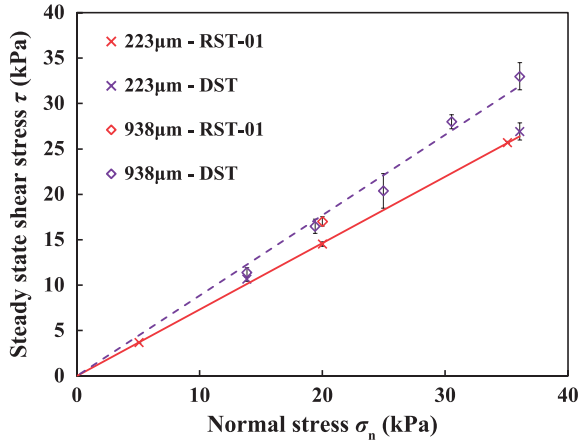

Fig. 14 Steady state locus (shear stress versus normal stress) of Eskal K0.1–0.5 (223 μm) and K0.5–0.8 (938 μm) using RST-01 and DST. The lines are the least mean square linear regression to the data with angle $\phi_{ss} = 36.2°$ for Eskal K0.1–0.5 and 41.5° for Eskal K0.5–0.8.

5.5 Summary of device comparison

In order to validate the consistency of the results obtained from different shear devices, we extrapolate the linearised yield loci and compare both angle of internal friction as well as cohesive strength (interception of linearised yield locus on y-axis) for the two reference powders (**Figs. 15** and **16**). The data from different shear testers are interpreted in different ways. In the case of the yield locus from the Jenike tester and DST, the shear points are linearised using a least square method, while the RST-01, RST-XS and FT4 are linearised using the default software with pro-rating method. For a free-flowing powder, Eskal150 (138 μm), we get a good agreement among the RST-01, the RST-XS and the FT4 for the cohesive strength, *c*, but higher values from the Jenike and es-

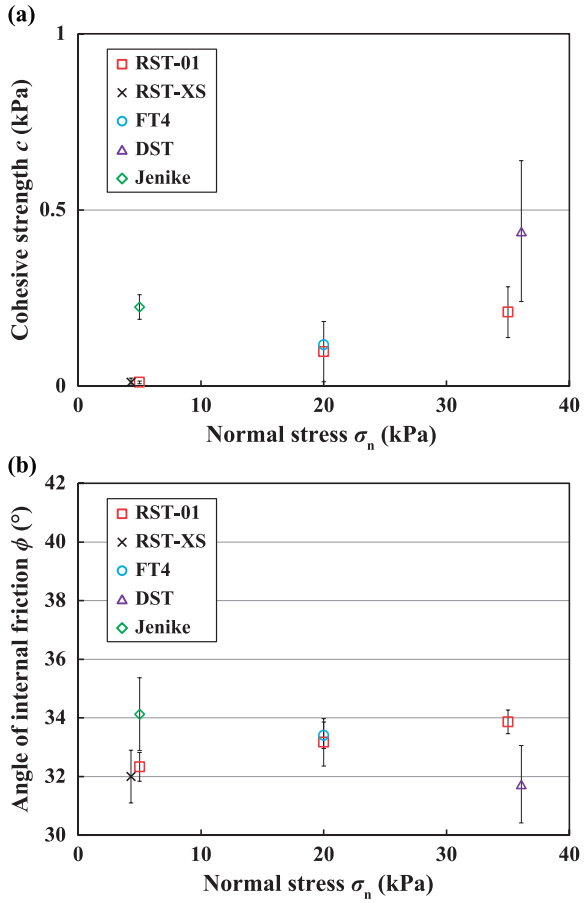

Fig. 15 **(a)** Cohesive strength, *c* and **(b)** angle of internal friction, ϕ, plotted against normal stress, σ_n, for Eskal150 (138 μm tested using all the devices in this study.

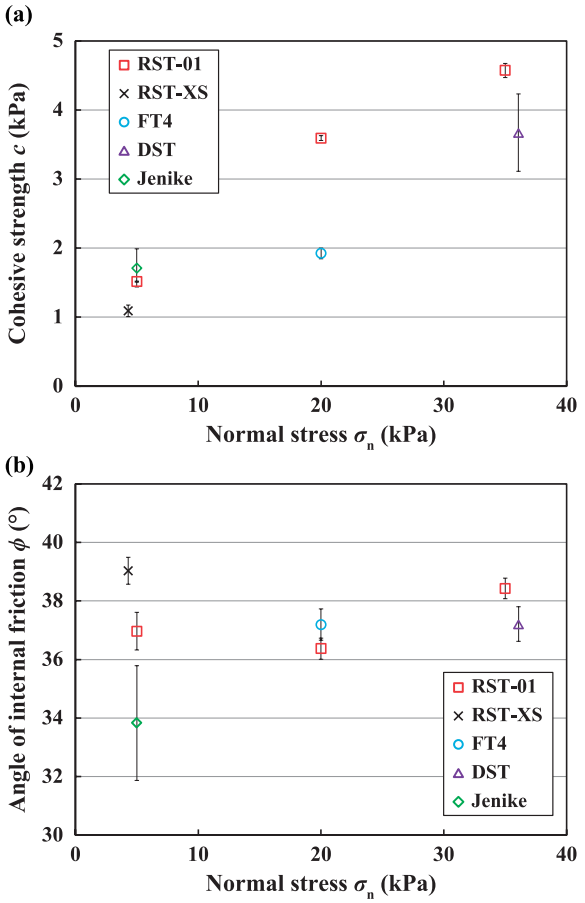

Fig. 16 **(a)** Cohesive strength, *c* and **(b)** angle of internal friction, ϕ, plotted against normal stress, σ_n, for Eskal300 (2.22 μm) tested using all the devices in this study.

pecially from the DST with also larger standard deviations (**Fig. 15(a)**). A similar observation is also found for the angle of internal friction as shown in **Fig. 15(b)**, but the ϕ value obtained from the DST is lower than the other devices. This is caused by the limit of the direct shear tester in the low stress range (below 1.0 kPa). The direct shear tester is initially designed for measuring the strength of soil samples in civil engineering, where the stresses applied are usually high, whereas our tests were performed at much lower stress levels, close to the accuracy limit (around 0.5 kPa) of the force ring on direct shear tester, resulting in a decrease in measurement accuracy for the direct shear tester using free-flowing powders. In the case of the Jenike shear tester, the ϕ value is higher than the other devices, but still within the deviation range.

In **Fig. 16**, we investigate the reproducibility of all the devices by looking at the most cohesive Eskal300 powder (2.22 µm). DST shows a good agreement with the highest standard deviation for cohesive strength, c, (**Fig. 16(a)**). However, the difference between the DST and the RST-01 is around 20 %. The RST-XS, Jenike and the RST-01 have a good agreement but FT4 shows a relatively lower value for c, thus underestimating the flowability of very cohesive powders. When we look at the ϕ value as shown in **Fig. 16(b)**, Jenike unexpectedly gives the lowest value with the highest standard deviation. The DST shows slightly lower values than the RST-01 and the FT4 has a good agreement with the RST-01 (within deviation range). Similar behaviour is observed for two other Eskal powders tested using RST-01, RST-XS, FT4 and DST: cohesive Eskal500 and easy-flowing Eskal15 (data are not shown here, see the **Tables** in Appendix B). Note that the vertical axes of cohesive strength are different in **Fig. 15** and **Fig. 16**.

6. Effects of varying particle size

In this section, we present the comparison of seven Eskal powders tested by the Schulze ring shear tester (RST-01) at different pre-shear stresses as given in **Table 3**. For the analysis of RST-01 data, we used the standard RST-CONTROL 95 software with "N-RHOB-correction" activated (Schulze, 2011). The powder have sizes ranging from 2.22 to 938 µm, and identical chemical composition as explained in **Table 1**. We characterize the above-mentioned seven powders in terms of bulk density, angle of internal friction, cohesive strength, steady state angle of internal friction, effective angle of internal friction and flow function.

6.1 Bulk density at steady state

As a first step, we look at the dependence of the bulk density on the normal stress and particle size for all the powders. Data are shown in **Fig. 17(a)**. Zero normal stress (arrows on bulk density axis) corresponds to the initial bulk density of the fresh samples before applying any stresses (provided by the manufacturer). By increasing normal stress, the bulk density increases for all powders with different rates, higher for small-particle-size powder and almost zero for Eskal80 (71 µm) and 150 (138 µm). However, for Eskal K0.1–0.5 (223 µm), the bulk density increases with increasing normal stress. We associate this trend to the wider particle size distribution (large span value 1.29 as shown in **Table 1**) and the visible huge amount of fines as shown in **Fig. 2**. A wider particle size distribution allows easy rearrangement of the packing structure when applying external load.

In **Fig. 17(b)**, we plot the bulk density with respect to

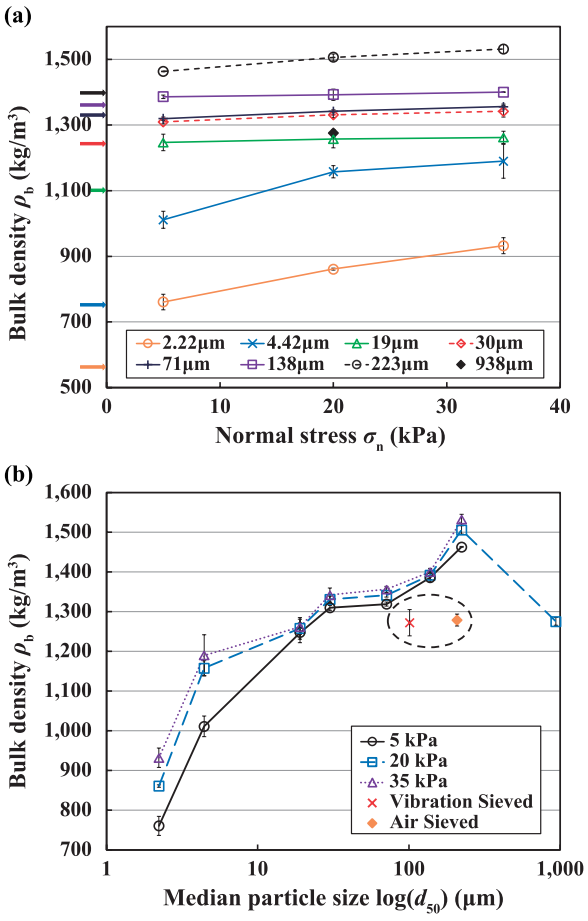

Fig. 17 Bulk density in steady state, ρ_b, plotted against **(a)** normal (pre-shear) stress, σ_n, **(b)** median particle size, d_{50}. Arrows represent the initial bulk density of the raw samples before stress and shear are applied. Symbols in the dashed area are sieved Eskal K0.1–0.5 (223 µm) sample sheared at $\sigma_n = 20$ kPa. Lines are guides to the eye.

the median particle size for different normal stresses. We observe an increasing trend with increasing particle size consistent for all normal stresses. This can be explained by the presence of cohesive forces (van der Waals) between primarily particles other than gravitational forces. Since Eskal powders are relatively dry, the presence of liquid bridging and other forces are expected to be small, the dry cohesive interaction will result in forming clusters and create many voids in the bulk, and therefore decrease the bulk density. As cohesive forces become smaller with increasing size, particles will have mainly frictional and gravitational forces without forming clusters and therefore the material can form a denser bulk solid. One extra powder, Eskal K0.5–0.8 (938 μm), is also tested under 20 kPa normal stress. This powder breaks the trend seen previously and shows a lower bulk density associated with the largest median particle size. In order to investigate further the role of the span in the bulk density behaviour, we perform sieving on the sample with largest span, Eskal K0.1–0.5 (223 μm). Two sieving methods are used: standard vibration sieving and high pressure air sieving. The median particle sizes reduce to 101 μm and 208 μm, in the case of vibration sieving and air sieving, respectively. The vibration sieving is only effective in removing the coarse particle but not the fines and thus leads to an increase of the span from 1.289 to 2.173. While the air sieving is effective enough to remove both coarse and fines and decrease the span to 0.395. The bulk densities for Eskal K0.1–0.5 (223 μm) after sieving are plotted in the dashed area of the same **Fig. 17(b)**. The bulk density of the sieved samples both decrease to values that are similar to the values of the largest median particle size powder, Eskal K0.5–0.8 (938 μm). This indicates that for a given median particle size, the span has a dominating effect on the bulk density of a powder.

6.2 Bulk responses from incipient and steady state flow

6.2.1 Angle of internal friction from incipient flow

The angle of internal friction describes the bulk friction during incipient flow of a powder, which is determined from the linearised yield locus as shown in **Fig. 8**. Although the yield locus for cohesive powder is non-linear by nature, the linearised yield locus can still be used to estimate the angle of internal friction in a certain stress range. This estimated value is one important property that determines the maximum bulk friction of a powder from a given pre-consolidation history. Here, unless specified, all angles of internal friction originate from linearised yield loci.

In **Fig. 18**, we plot the angle of internal friction against normal stress at three different pre-shear normal stress and particle size for the 7 powders studied (Eskal K0.5–0.8 is also included here but with only one point). Within the stresses investigated, there is no apparent dependence of the angle of internal friction on the normal stress (**Fig. 18(a)**). However, if we focus on the dependence on the particle size as shown in **Fig. 18(b)**, we observe that when d_{50} is lower than approximately 30 μm, ϕ decreases with increasing particle size. Then, for $30 < d_{50} < 150$ μm, we observe that the ϕ is almost constant with changing particle size for the three pre-shear normal stresses chosen. Interestingly, if the particle size keeps rising to $d_{50} < 150$ μm, ϕ follows a parallel rise and achieves similar values to the ones obtained for samples smaller than 30 μm. For Eskal K0.1–0.5 ($d_{50} = 223$ μm), the angle of internal friction increases back to around 38°.

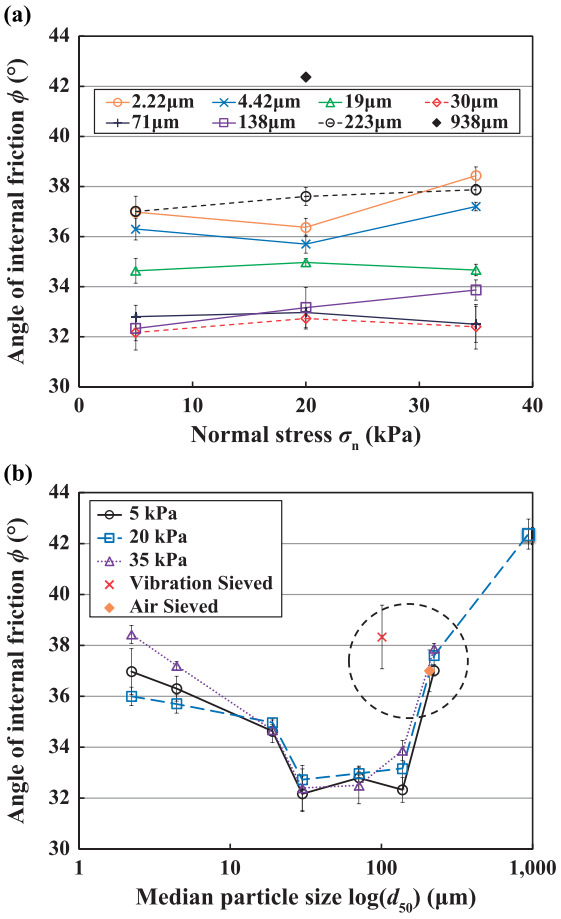

Fig. 18 Angle of internal friction, ϕ, plotted against **(a)** pre-shear normal stress, σ_n, **(b)** median particle size, d_{50}. Symbols in the dashed area are sieved Eskal K0.1–0.5 (223 μm) sample sheared at $\sigma_n = 20$ kPa. Lines are guides to the eye.

We have run several tests/checks with the goal of elucidating the non-monotonic behavior that observed in **Fig. 18(b)**. First, we further test another sample in the range of $d_{50} > 150$ μm, namely Eskal K0.5–0.8 ($d_{50} = 938$ μm), at 20 kPa pre-shear stress. The ϕ value of Eskal K0.5–0.8 increases even further to around 42°. This confirms that the increasing trend is not limited only to a

specific sample. As second step, we have measured the angle of internal friction for the two sieved samples obtained after sieving Eskal K0.1–0.5 (223 µm) via vibration and air methods that are already introduced in Sec. 6.2.1. While the bulk density strongly reduces after sieving, the angle of internal friction remains unaffected as shown in the dashed area of **Fig. 18(b)**, which indicates that the span of particle size distribution is not the primary factor influencing the bulk friction. Finally, in order to check the influence of the devices, we have further tested Eskal K0.1–0.5 (223 µm) and K0.5–0.8 (938 µm) in the direct shear tester (DST), and the results are reported in **Fig. 14**. The flow behaviour of both powders are very similar using RST-01 and DST. This agreement clarifies that the behaviour originates from material properties rather than from a specific shear device.

One possible explanation of this interesting behaviour on bulk friction would be that the different size particles have a similar shape (this is visible by comparing the roundness between Eskal K0.1–0.5 and K0.5–0.8 in **Table 1**) but different surface roughness/asperity, but this has to be further investigated and it is far beyond the scope of this study. Another possibility is the competition between the inter-particle cohesion and inter-particle friction (caused by shape). When the particles are small, the inter-particle cohesion dominates the flow behaviour and enhances the shear resistance. Also when a sample is confined under a given confining stress, if the inter-particle cohesion is high, the sample bulk density will be low, which gives more free spaces for particles to move around. Therefore, the geometrical interlocking does not play an important role here. When the particle size is large, we have almost no influence from inter-particle cohesion and the whole powder is more densely packed, so that the inter-particle friction/interlocking (shape/geometry) is the ruling mechanism of the bulk friction behaviour. For an intermediate particle size, these two effects are both reducing but still competing with each other, and they cannot be distinguished.

6.2.2 Cohesive strength from incipient flow

As a complement to the angle of internal friction, one has to also look at the cohesive strength, which is the extrapolated intercept from the linearised yield locus, and gives an indication of the strength of the powder under zero confining stress (σ_n). In **Fig. 19(a)**, we plot the cohesive strength against the pre-shear normal stress. As expected, the values of cohesive strength at given stress levels are higher for powders with finer particle size. The cohesive strength of all powders increases with increasing normal stress, but with different slopes. The cohesive strength of the two finest powders, Eskal300 (2.22 µm) and Eskal500 (4.42 µm), increase conspicuously with normal stress.

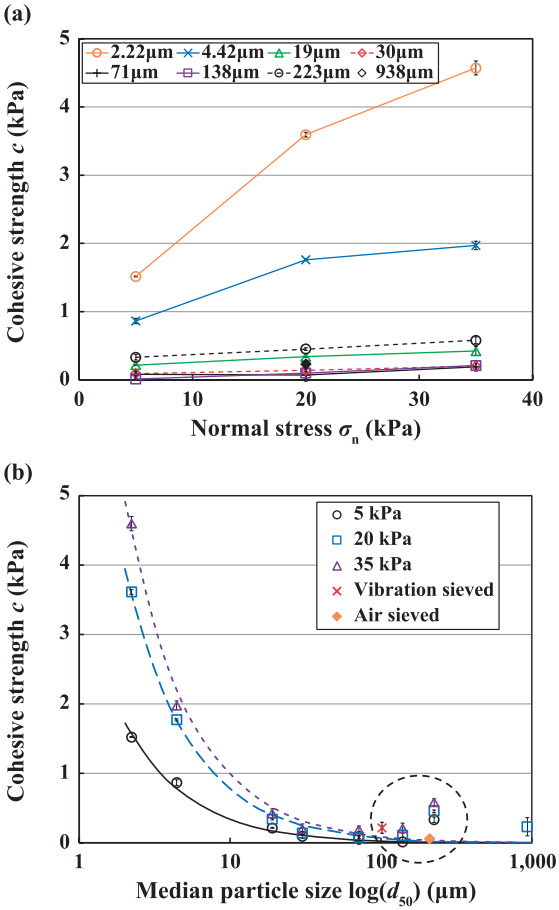

Fig. 19 Cohesive strength, c, plotted against **(a)** pre-shear normal stress, σ_n, **(b)** median particle size, d_{50}. Symbols in the dashed area are sieved Eskal K0.1–0.5 (223 µm) sample sheared at $\sigma_n = 20$ kPa. Lines are from the fitted function: $c(d_{50}) = \sigma_{pre} * d_c/d_{50}$ with d_c = 0.6919, 0.3953 and 0.2809 µm for σ_{pre} = 5, 20 and 35 kPa, repectively.

As we focus on the particle size dependence in **Fig. 19(b)**, we see a monotonically decreasing bulk cohesion with increasing particle size for all the normal stress levels investigated. However, the cohesive strength for raw Eskal K0.1–0.5 (223 µm) increases above this trend (as shown in the dashed area in the figure). This apparent discrepancy was also observed in the bulk density and the angle of internal friction, as explained earlier. We further investigated this behaviour by sieving the sample using different techniques. It seems that our air sieving procedures are effective and reduce the cohesive strength of the powder by separating the fines from the coarse fractions. The theory that smaller particles have the strongest cohesive forces, acting most effectively on each other, is consistent with the strongest decrease in cohesion for the air-sieved samples in which the fines are most effectively removed. The observation of removing fines reduces bulk cohesion but does not affect bulk friction supports the hypothesis that frictional flow behaviour of powders in the

range of $d_{50} > 150$ μm is governed by particle interlocking.

In **Fig. 19(b)**, we have also given fitted lines based on the equation as shown in the caption. All our data fitted well with a power law dependence and this power has its origin from the adhesive forces between two particles, as introduced by Rumpf in 1990 (Rumpf 1990, Rabinovich et al. 2000), where the adhesion force between two particles is linearly proportional to particle diameter: $F_{ad} \propto d$. While for the cohesive strength, it is a bulk property with an unit of stress. Therefore, cohesive strength is proportional to the adhesion force divided by effective contact area: $c \propto F_{ad}/d^2$, and finally we get $c \propto d^{-1}$, which is the relation used for our fitting.

6.2.3 Bulk friction from steady state flow

Along with the bulk density (volume fraction), angle of internal friction and cohesive strength, the steady state angle of internal friction, ϕ_{ss}, also plays a major role in determining the powder flow behaviour. The steady state flow does not depend on time change or sample history and one could get a unique bulk friction response to shearing for each normal stress level for a given sample. We first look at the ϕ_{ss} with respect to the applied normal stress in **Fig. 20(a)**. For samples with median particle size higher than 20 μm (Eskal30, 80, 150 and K0.1–0.5), the ϕ_{ss} behaves similarly as ϕ, no clear dependence on normal stress is observed. However, for samples smaller than 20 μm (Eskal300, 500 and 15), ϕ_{ss} decreases with increasing normal stress.

When we look at the size influence on ϕ_{ss} in **Fig. 20(b)**, we observe a very similar trend to the angle of internal friction in **Fig. 18(b)**. However, the value of ϕ_{ss} for largest size powder is lower than the value of the finest powder, where ϕ of the coarsest powder exceeds the finest. This indicates that the inter-particle cohesion contributes more to the shear resistance at steady state flow than at incipient flow. When looking at the behaviour of the two sieved samples, ϕ_{ss} stay almost unchanged after sieving, which is consistent with **Fig. 18(b)**.

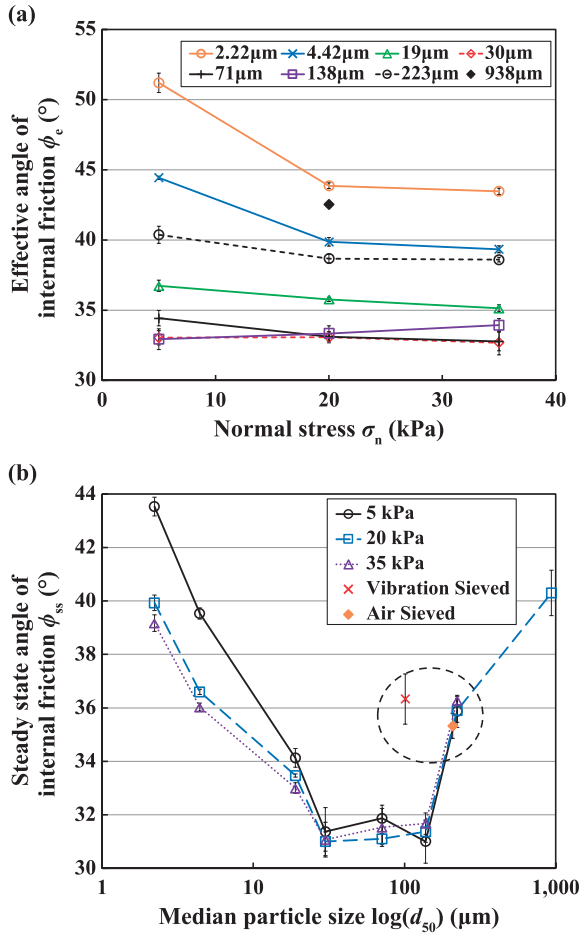

Fig. 20 Steady state angle of internal friction, ϕ_{ss}, plotted against **(a)** pre-shear normal stress, σ_n, **(b)** median particle size, d_{50}. Symbols in the dashed area are sieved Eskal K0.1–0.5 (223 μm) sample sheared at $\sigma_n = 20$ kPa. Lines are guides to the eye.

6.3 Quantities relevant for silo design

The parameters mentioned in the sections above are determined directly from the physical response of powders in the shear tester, e.g., bulk friction values can be directly calculated from the measured normal and shear stresses, and are very useful for understanding the powder's physical behaviour. However, for designing a silo, some additional parameters play an important role (Jenike, 1976; Schulze, 2008, 2014b). These will be discussed in the following sections.

6.3.1 Effective angle of internal friction

The effective angle of internal friction is defined as the angle of the effective yield locus, which is the line starting at the origin of the $\sigma_n - \tau$ plane and tangent to the Mohr circle (see **Fig. 8**). And this property is crucial for designing the hopper angle in order to achieve mass flow in a silo.

In **Fig. 21**, the effective angle of internal friction is plotted against the normal stress and median particle size. Within the stress levels investigated, ϕ_e decreases with increasing normal stress, except for two intermediate size powders—Eskal30 (30 μm) and 150 (138 μm), which shows a consistent behaviour with ϕ_{ss} independent of the normal stress. Interestingly, for even higher particle size, Eskal K0.1–0.5 (223 μm), ϕ_e again decreases with applied normal stress.

When we focus on the dependence of the effective angle of internal friction on the particle size as shown in **Fig. 21(b)**, we observe a very similar trend as ϕ and ϕ_{ss}, especially with values of ϕ_e consistently higher than ϕ_{ss} for both very fine and very coarse powders. Also in this

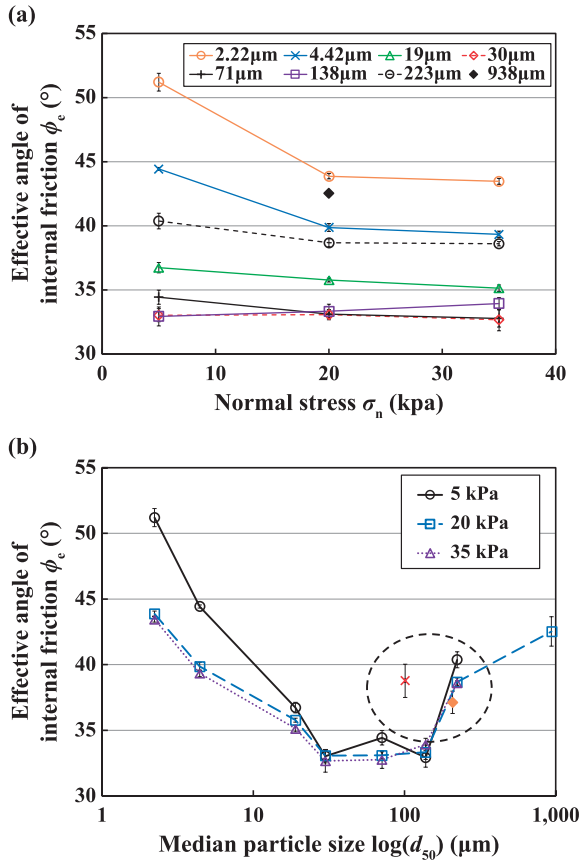

Fig. 21 Effective angle of internal friction, ϕ_e, plotted against **(a)** pre-shear normal stress, σ_n, **(b)** median particle size, d_{50}. Symbols in the dashed area are sieved Eskal K0.1–0.5 (223 μm) sample sheared at $\sigma_n = 20$ kPa. Lines are guides to the eye.

case, sieving barely affects the behaviour of the powders, see dashed area in **Fig. 21(b)**.

6.3.2 Flow function and powder flowability

Finally, we process the results to look at the powder flowability in the form of the flow function to evaluate how a given powder would fail/flow under a given major consolidation stress (see **Fig. 8**). This is also of great significance for designing the outlet diameter of a silo (Schulze, 2014a). When a powder sample is compressed in a confined geometry, e.g. a cylinder in a uni-axial tester, the major consolidation stress is named as σ_1, which indicates the maximum compressive stress achieved in the sample. If the powder is sufficiently cohesive, it will form an intact bulk/block after the confinement is removed. If the block is compressed again, the minimum stress needed to achieve sample failure/breakage is called the unconfined yield strength, σ_c. Note that the sample stress paths in uni-axial testers and shear testers are different, but the stress states could be linked using Mohr's Circle. The curve $\sigma_c = f(\sigma_1)$ is called flow function in powder engineering, which can be used to characterize material

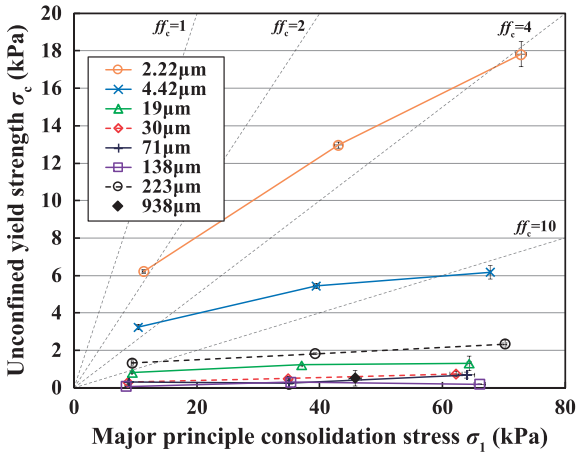

Fig. 22 Flow function: unconfined yield strength, σ_c, plotted against major consolidation stress, σ_1 under 3 different pre-shear stresses using RST-01. Different symbols/colours represent different materials. Note that for Eskal K0.5–0.8, there is only one point, and we have error bars with both σ_c and σ_1. Lines are guides to the eye.

flowability, $ff_c = \sigma_1/\sigma_c$ (Schulze, 2008). The flowability is defined as follows:

- $ff_c < 1$ not flowing
- $1 < ff_c < 2$ very cohesive
- $2 < ff_c < 4$ cohesive
- $4 < ff_c < 10$ easy flowing
- $ff_c > 10$ free flowing

In **Fig. 22**, we plot the flow functions for 7 limestone powders. As we can see, our powders cover almost the whole range of flowability, from cohesive to free flowing. In the stress range we investigated, σ_c increases for all the samples with increasing σ_1. As expected, the slope of the increase trend becomes higher with decreasing particle size, with the maximum slope of Eskal300 (minimum particle size). The flowability of a certain powder depends not only on the major consolidation stress σ_1, but also on particle size.

7. Conclusion and outlook

In this study, we have systematically examined the powder flow behaviour of limestone powder samples with varying median particle sizes in different shear testers at different confining stress levels. The major goal is to understand the relation between microscopic properties such as particle size and contact cohesion and macroscopic, bulk properties such as bulk density, cohesive strength and shear resistance (characterized by the effective angle of internal friction, the internal friction at steady state flow, and the internal friction).

All shear testers investigated show highly repeatable/

reproducible results and good overall, consistent agreement among each other. Direct shear devices (Jenike and ELE direct shear tester) give the highest standard deviations. The yield loci obtained by the Schulze ring shear tester (RST-01) are consistently slightly higher than the results from other testers, which, on the practical side, results in a more conservative but safer silo design. The shear protocol evidently influences the measurements as shown by comparing the RST-01 and the FT4, where the latter gives a significantly lower yield locus, which we attribute to a different pre-shear protocol. As a conclusion, while the automated devices minimize the operator influence, the output should be carefully interpreted, as differences in the protocol can result in considerable deviations in the measured material response even if the qualitative trends are found to be consistent among different testers.

In order to study the material behaviour, eight limestone powders with identical chemical composition and median particle size ranging from 2.2 µm to 938 µm have been tested in a wide range of normal stresses (5, 20 and 35 kPa). Both factors, size and stress, are found to influence the bulk flow significantly. As expected, the bulk density and cohesive strength increase with increasing normal stress, the effect being stronger for finer particles. On the other hand, the angle of internal friction seems to be unaffected by the normal stress (at least in the range investigated here), while the effective angle of internal friction and the steady state angle of internal friction show a decreasing trend with normal stress.

When we look at the dependence of the macroscopic flow on particle size, two regimes can be distinguished, above and below the median particle size of about 150 µm. For the fine particle regime, contact cohesion dominates the bulk behaviour, the effect getting smaller with increasing particle size. The bulk density increases monotonically with particle size, and the bulk cohesion (cohesive strength) decreases to nearly zero. The friction angles (effective angle of internal friction, angle of internal friction and steady state angle of internal friction), follow a similar decreasing trend as bulk cohesion.

In the coarse particle regime (150 to 938 µm), the bulk behaviour is less obvious. The bulk cohesion slightly increases while bulk density increases, then decreases. The bulk friction angles increase with increasing particle size up to values comparable to those of the finest powders. In order to check the effect of small particles in this regime, fines are removed from the coarse samples via air sieving. This results in a significant reduction in bulk density and bulk cohesion, while the bulk friction angles are barely affected. This proves that the fine particles being the main source of cohesion. The competition between contact cohesion and geometrical effects can explain the transition between the two regimes. For dry powders consisting of large particles, the inter-particle cohesive forces, especially the van der Waals forces, become negligible. The interlocking between particles due to the surface roughness and shape dominates the bulk behaviour of coarse samples, while cohesion is the key contribution that governs the shear strength of fine powders. The geometrical interlocking effect is further enhanced by the increase of the bulk density for coarse samples. On the other hand, low density is associated with small median particle size, due to the presence of clusters and large pores.

For the sake of completeness, we also look at the flow behaviour of our powders, as relevant for the silo-design procedure. Overall, the flowability increases when increasing normal stress (powders become more free flowing) for finer samples, with the effect becoming weaker for coarse samples that are more free flowing anyway.

The present paper is the beginning of a collection of experimental data that, in the future, can be enriched with more data from many more materials of both industrial and academic interest. Our speculations on the interesting bulk cohesion and friction behaviour with increasing particle size have to be further investigated. Furthermore, this experimental database can be used as a source for design (e.g. silo) procedures and as a benchmark for further experimental studies. Last but not least, the development, calibration and validation of particle models and simulations, especially the DEM contact models, and simulations of element tests (shear tests), require experimental data as presented here.

Acknowledgement

Helpful discussions with Abhinendra Singh and Bert Scheper as well as the help from Bruno E. Chávez Montesareon on experimental set-ups are gratefully acknowledged. This work is financially supported by the T-MAPPP project of the European-Union-funded Marie Curie Initial Training Network FP7 (ITN607453); see http://www.t-mappp.eu/ for more information.

Nomenclature

ρ_p	Particle density (kg/m^3)
ρ_0	Initial bulk density (kg/m^3)
ρ_b	Bulk density (kg/m^3)
w	Moisture content (%)
d_{10}	Particle diameter where 10 % of distribution is below this value (µm)
d_{50}	Particle median size where 50 % of distribution is below this value (µm)

d_{90}	Particle diameter where 90 % of distribution is below this value (μm)
Ψ	Roundness ([–])
τ	Shear stress (kPa)
τ_{ss}	Steady state shear stress (kPa)
τ_p	Peak failure shear stress (kPa)
σ_n	Normal stress (kPa)
σ_{pre}	Pre-shear normal stress (kPa)
c	Cohesive strength of yield locus or bulk cohesion (kPa)
c_{ss}	Cohesive strength of steady state locus (kPa)
σ_c	Unconfined yield strength (kPa)
σ_1	Major consolidation stress (kPa)
σ_2	Minor consolidation stress (kPa)
ϕ	Angle of internal friction (°)
ϕ_e	Effective angle of internal friction (°)
ϕ_{ss}	Steady state angle of internal friction (°)
ff_c	Flowability ([–])

References

Akers R.J., The certification of a limestone powder for Jenike shear testing (CRM 116), *EUR (Luxembourg)*, 1992.

Alonso-Marroquin F., Herrmann, H.J., Ratcheting of granular materials, Physics Review Letter, 92 (2004) 54301.

Alshibli K.A., Sture, S., Shear band formation in plane strain experiments of sand, Journal of Geotechnical and Geoenvironmental Engineering, 126 (2000) 495–503.

ASTM-D6128-16, Standard test method for shear testing of bulk solids using the Jenike shear cell, West Conshohocken, PA: ASTM International, 2006.

ASTM-D6773-16, Standard shear test method for bulk solids using the Schulze ring shear tester, West Conshohocken, PA: ASTM International, 2008.

ASTM-D7891-15, Standard test method for shear testing of powders using the freeman technology FT4 powder rheometer shear cell, West Conshohocken, PA: ASTM International, 2015.

Bardet J.P., Experimental Soil Mechanics, Prentice-Hall, Upper Saddle River, New Jersey, 1997.

Berry R.J., Bradley M.S.A., McGregor R.G., Brookfield powder flow tester-Results of round robin tests with CRM-116 limestone powder, Proceedings of the Institution of Mechanical Engineers, Part E: Journal of Process Mechanical Engineering, 229 (2015) 215–230.

Bi D., Zhang J., Chakraborty B., Behringer R.P., Jamming by shear, Nature, 480 (2011) 355–358.

Carr J.F., Walker D.M., An annular shear cell for granular materials, Powder Technology, 1 (1968) 369–373.

Casagrande A., The determination of the pre-consolidation load and its practical significance, Proceedings of the international conference on soil mechanics and foundation engineering, 3 (1936) 60–64.

Cates M.E., Haw M.D., Holmes C.B., Dilatancy, jamming, and the physics of granulation, Journal of Physics: Condensed Matter, 17 (2005) S2517.

Cundall P.A., Numerical experiments on localization in frictional materials, Ingenieur-Archiv, 59 (1989) 148–159.

Feise H.J., A review of induced anisotropy and steady-state flow in powders, Powder Technology, 98 (1998) 191–200.

Feise H., Schwedes J., Investigation of the Behaviour of Cohesive Powder in the Biaxial Tester, KONA Powder Particle Journal, 13 (1995) 99–104.

Fitzpatrick J.J., Barringer S.A., Iqbal T., Flow property measurement of food powders and sensitivity of Jenike's hopper design methodology to the measured values, Journal of Food Engineering, 61 (2004) 399–405.

Freeman R., Measuring the flow properties of consolidated, conditioned and aerated powders—A comparative study using a powder rheometer and a rotational shear cell, Powder Technology, 174 (2007) 25–33.

Freeman R.E., Cooke J.R., Schneider L.C.R., Measuring shear properties and normal stresses generated within a rotational shear cell for consolidated and non-consolidated powders, Powder Technology, 190 (2009) 65–69.

GDR-MiDi, On dense granular flows, European Physical Journal E–Soft Matter, 14 (2004) 341–365.

Harder J., Schwedes J., The development of a true biaxial shear tester, Particle & Particle Systems Characterization, 2 (1985) 149–153.

Imole O.I., Paulick M., Magnanimo V., Morgeneyer M., Montes B.E., Ramaioli M., Kwade A., Luding S., Slow stress relaxation behavior of cohesive powders, Powder Technology, 293 (2016) 82–93.

Janssen R.J.M., Zetzener H., Measurements on cohesive powder with two biaxial shear testers, Chemical Engineering & Technology, 26 (2003) 147–151.

Jenike A.W., Storage and Flow of Solids, Bulletin No. 123, Bulletin of the University of Utah, 53 (1964).

Jenike A.W., Quantitative design of mass-flow bins, Powder Technology, 1 (1967) 237–244.

Jenike A.W., Storage and flow of solids. bulletin no. 123, vol. 53, no. 26, November 1964, Technical report, Utah University, Salt Lake City (USA), 1976.

Kamath S., Puri V.M., Manbeck H.B., Flow property measurement using the Jenike cell for wheat flour at various moisture contents and consolidation times, Powder Technology, 81 (1994) 293–297.

Kamath S., Puri V.M., Manbeck H.B., Hogg R., Flow properties of powders using four testers-measurement, comparison and assessment, Powder Technology, 76 (1993) 277–289.

Koynov S., Glasser B., Muzzio F., Comparison of three rotational shear cell testers: Powder flowability and bulk density, Powder Technology, 283 (2015) 103–112.

Kumar N., Luding S., Memory of jamming–multiscale models for soft and granular matter, Granular Matter, 18 (2016) 1–21.

Liu A.J., Nagel S.R., Nonlinear dynamics: Jamming is not just cool any more, Nature, 396 (1998) 21–22.

Luding S., Anisotropy in cohesive, frictional granular media, Journal of Physics: Condensed Matter, 17 (2005a) S2623–S2640.

Luding S., Shear flow modeling of cohesive and frictional fine powder, Powder Technology, 158 (2005b) 45–50.

Luding S., Cohesive, frictional powders: contact models for tension, Granular Matter, 10 (2008) 235–246.

Luding S., Granular matter: So much for the jamming point, Nature, 12 (2016) 531–532.

Majmudar T.S., Behringer R.P., Contact force measurements and stress-induced anisotropy in granular materials, Nature, 435 (2005) 1079–1082.

Morgeneyer M., Brendel L., Farkas Z., Kadau D., Wolf D.E., Schwedes J., Can one make a powder forget its history?, Proceedings of the 4th international conference for conveying and handling of particulate solids, Budapest, 2003, pp. 12–118.

Morgeneyer M., Schwedes J., Investigation of powder properties using alternating strain paths, Task Quarterly, 7 (2003) 571–578.

Rabinovich Y.I., Adler J.J., Ata A., Singh R.K., Moudgil B.M., Adhesion between nanoscale rough surfaces: I. Role of asperity geometry, Journal of Colloid and Interface Science, 232 (2000) 10–16.

Radjai F., Jean M., Moreau J.J., Roux S., Force distribution in dense two-dimensional granular systems, Physical Review Letters, 77 (1996) 274–277.

Radjai F., Roux S., Moreau J.J., Contact forces in a granular packing, Chaos: An Interdisciplinary Journal of Nonlinear Science, 9 (1999) 544–550.

Rumpf H., Particle technology, Chapman & Hall, London/New York, 1990.

Russell A., Müller P., Shi H., Tomas J., Influences of loading rate and preloading on the mechanical properties of dry elasto-plastic granules under compression, AIChE Journal, 60 (2014) 4037–4050.

Salehi H., Barletta D., Poletto M., A comparison between powder flow property testers, Particuology, 32 (2017) 10–20.

Savage S.B., Hutter K., The motion of a finite mass of granular material down a rough incline, Journal of Fluid Mechanics, 199 (1989) 177–215.

Schulze D., Entwicklung und Anwendung eines neuartigen Ringschergerätes, Aufbereitungs-Technik, 35 (1994) 524–535.

Schulze D., Flow properties of bulk solids (v), Deutsche Keramische Gesellschaft und Nederlandse Keramische Vereniging, Annual Meeting 2002, Eindhoven., 2002, pp. 21–23.10.

Schulze D., Time- and velocity-dependent properties of powders effecting slip-stick oscillations, Chemical Engineering & Technology, 26 (2003a) 1047–1051.

Schulze D., Towards more reliability in powder testing (v), Proceedings of the 4th international conference for conveying and handling of particulate solids (CHoPS), Budapest, 2003b, pp. 5–31.

Schulze D., Powders and bulk solids: behavior, characterization, storage and flow, Springer, 2008.

Schulze D., Round robin test on ring shear testers, Advanced Powder Technology, 22 (2011) 197–202.

Schulze D., Beispiele gemessener Fließeigenschaften, in 'Pulver und Schüttgüter', Springer, 2014a, pp. 249–268.

Schulze D., Verfahrenstechnische Siloauslegung, in 'Pulver und Schüttgüter', Springer, 2014b, pp. 335–360.

Schwedes J., Vergleichende Betrachtungen zum Einsatz von Schergeräten zur Messung von Schüttguteigenschaften, Proceedings of PARTEC, Nürnberg, 1979, pp. 278–300.

Schwedes J., Review on testers for measuring flow properties of bulk solids, Granular Matter, 5 (2003) 1–43.

Schwedes J., Schulze D., Measurement of flow properties of bulk solids, Powder Technology, 61 (1990) 59–68.

Shibuya S., Mitachi T., Tamate S., Interpretation of direct shear box testing of sands as quasi-simple shear, Geotechnique, 47 (1997) 769–790.

Singh A., Magnanimo V., Saitoh K., Luding S., Effect of cohesion on shear banding in quasistatic granular materials, Physical Review E, 90 (2014) 022202.

Teunou E., Fitzpatrick J.J., Synnott E.C., Characterisation of food powder flowability, Journal of Food Engineering, 39 (1999) 31–37.

Thakur S.C., Ahmadian H., Sun J., Ooi J.Y., An experimental and numerical study of packing, compression, and caking behaviour of detergent powders, Particuology, 12 (2014) 2–12.

Tomas J., Product design of cohesive powders – Mechanical properties, compression and flow behavior, Chemical Engineering & Technology, 27(6) (2005) 605–618.

Tsunakawa H., Aoki R., Measurements of the failure properties of granular materials and cohesive powders, Powder Technology, 33 (1982) 249–256.

Van Hecke M., Jamming of soft particles: geometry, mechanics, scaling and isostaticity, Journal of Physics: Condensed Matter, 22 (2009) 033101.

Witt W., Altrogge D., Rutsch O., High speed image analysis and dispersion for size and shape characterisation on fibres, Proceedings of 5th World Congress of Particle Technology, 2006.

Wolf B., Scirocco R., Frith W.J., Norton I.T., Shear-induced anisotropic microstructure in phase-separated biopolymer mixtures, Food Hydrocolloids, 14 (2000) 217–225.

Yang Y., Fei W., Yu H.-S., Ooi J., Rotter M., Experimental study of anisotropy and non-coaxiality of granular solids, Granular Matter, 17 (2015) 189–196.

Zetzener, H. Schwedes, J., Relaxation and creep of dry bulk solids, Particle & Particle Systems Characterization, 19 (2002) 144–148.

Appendix A. Test details on yield locus and steady state locus

Table A1 Summary of pre-shear/shear normal stress values used in each shear device to measure yield locus.

Device	Samples	Normal stress applied (kPa)
RST-01	Eskal 300, 500, 15, 30, 80, 150, K0.1–0.5	Pre-shear at 5 Shear at 0.5, 1, 1.5, 2, 3
	Eskal 300, 500, 15, 30, 80, 150, K0.1–0.5, K0.5–0.8	Pre-shear at 20 Shear at 2, 5, 8, 12, 16
	Eskal 300, 500, 15, 30, 80, 150, K0.1–0.5	Pre-shear at 35 Shear at 2, 5, 10, 15, 20
RST-XS	Eskal 300, 500, 15, 150	Pre-shear at 4.3 Shear at 0.35, 0,85, 1.4, 2.1, 3.6
DST	Eskal 300, 500, 15, 150	Pre-shear at 36.1 Shear at 1.4, 13.9, 19.4, 25, 30.5
FT4	Eskal 300, 500, 15, 150	Pre-shear at 20 Shear at 0.1, 0.5, 1, 2, 5, 8, 16
Jenike	Eskal 300, 150	Pre-shear at 5 Shear at 0.5, 1.5, 3

Table A2 Summary of normal stress values applied using direct shear tester (DST) to measure steady state locus.

Samples	Normal stress applied (kPa)
Eskal 300, 500, 15, 150	1.4, 2.8, 4.2, 5.5, 6.9, 8.2, 9.6, 11, 12.3, 13.9, 19.4, 25, 30.5, 36.1
Eskal K0.1–0.5	13.9, 36.1
Eskal K0.5–0.8	13.9, 19.4, 25, 30.5, 36.1

Appendix B. Test results of all the powders and devices shown in this paper

Table B1 Data measured from RST-01 for several Eskal powders and different pre-shear stresses.

Device	Sample	d_{50} (μm)	σ_{pre} (kPa)	c (kPa)	σ_1 (kPa)	σ_c (kPa)	ρ_b (kg/m^3)	ϕ_e (°)	ϕ (°)	ϕ_{ss} (°)
RST-01	K0.5–0.8	938	5	0.08	11.49	0.33	1288.00	41.37	40.57	38.97
			20	0.23	45.77	0.51	1275.67	42.53	42.37	40.30
			35	0.06	88.49	0.27	1299.67	42.30	42.23	41.20
	K0.1–0.5	223	5	0.33	9.47	1.33	1463.33	40.37	37.00	35.87
			20	0.45	39.23	1.82	1506.00	38.67	37.60	35.90
			35	0.58	70.17	2.33	1531.67	38.60	37.87	36.27
	Eskal150	138	5	0.01	8.53	0.06	1386.00	32.93	32.22	31.00
			20	0.10	35.34	0.31	1392.33	33.33	33.17	31.37
			35	0.21	66.07	0.19	1400.33	33.93	33.87	31.67
	Eskal80	71	5	0.08	8.88	0.31	1319.33	34.43	32.80	31.87
			20	0.07	35.02	0.25	1341.67	33.10	32.97	31.10
			35	0.19	63.9	0.68	1356.33	32.77	32.50	31.53
	Eskal30	30	5	0.09	8.83	0.31	1309.67	33.03	32.17	31.37
			20	0.14	34.84	0.49	1331.00	33.07	32.73	31.00
			35	0.20	62.20	0.74	1342.00	32.67	32.40	31.07
	Eskal15	19	5	0.21	9.44	0.82	1247.00	36.73	34.63	34.13
			20	0.34	37.08	1.23	1257.67	35.77	34.97	33.77
			35	0.42	64.34	1.31	1262.00	35.13	34.67	33.00
	Eskal500	4.42	5	0.86	10.47	3.25	1011.33	44.43	36.30	39.53
			20	1.76	39.45	5.44	1157.67	39.87	35.70	36.60
			35	1.97	67.79	6.17	1190.00	39.33	37.20	36.03
	Eskal300	2.22	5	1.52	11.33	6.21	760.67	51.20	36.97	43.53
			20	3.59	43.06	12.97	861.00	43.87	36.37	39.93
			35	4.57	72.81	17.82	932.33	43.47	38.43	39.17

Table B2 Data measured from RST-XS, FT4 and DST for several Eskal powders and different pre-shear stresses.

Device	Sample	d_{50} (μm)	σ_{pre} (kPa)	c (kPa)	σ_1 (kPa)	σ_c (kPa)	ρ_b (kg/m^3)	ϕ_e (°)	ϕ (°)	ϕ_{ss} (°)
RST-XS	Eskal150	138	4.3	0.01	7.67	0.13	1447.67	34.13	32.00	29.93
	Eskal15	19		0.07	7.91	0.26	1416.67	34.57	33.80	32.53
	Eskal500	4.42		0.41	8.70	0.93	1015.00	40.83	38.33	37.50
	Eskal300	2.22		1.09	9.39	4.16	767.67	50.90	39.03	42.97
FT4	Eskal150	138	20	0.12	30.88	0.43	1441.45	33.75	33.41	24.91
	Eskal15	19		0.20	32.57	0.75	1297.10	33.51	32.95	29.82
	Eskal500	4.42		0.75	36.68	2.94	1081.57	37.59	35.68	34.16
	Eskal300	2.22		1.92	41.06	7.75	782.16	41.82	37.20	38.21
DST	Eskal150	138	36.08	0.86	59.83	1.95	1429.09	32.61	31.00	31.22
	Eskal15	19		1.30	60.83	3.10	1281.59	35.83	34.08	34.91
	Eskal500	4.42		2.13	61.33	7.40	1204.08	37.60	34.61	35.24
	Eskal300	2.22		3.67	64.47	10.07	952.30	42.01	37.21	38.27
Jenike	Eskal150	138	5	0.22	18.17	0.35	1445.63	35.31	34.13	32.09
	Eskal300	2.22		1.71	11.30	7.17	788.91	47.95	33.83	37.95

Appendix C. The explanation on the graphical abstract

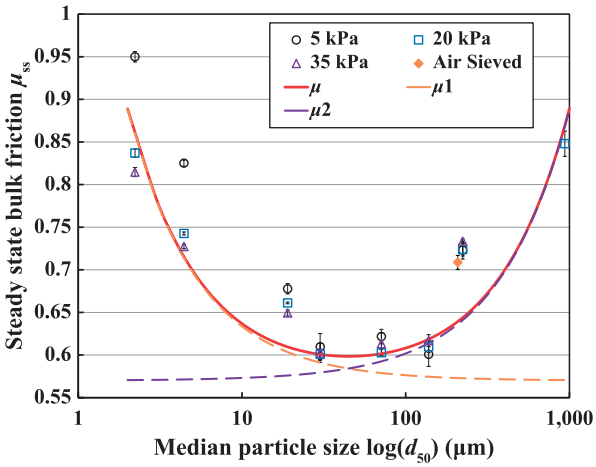

Fig. C1: Steady state bulk friction, $\mu_{ss} = \tan(\phi_{ss})$, plotted against median particle size, d_{50}. Solid line is the fitted function, μ, in Eq. (1C). Orange and purple dashed lines represent contributions from inter-particle cohesion and geometrical/inter-locking, respectively.

In Fig. C1, we have plotted the same data as shown in Fig. 20(b), but with a proposed theory which fits the data with $\sigma_{pre} = 20$ kPa:

$$\mu = \mu_0 \left(1 + \frac{d_{c\mu}}{d_{50}} + \frac{d_{50}}{d_{g\mu}}\right) \tag{1C}$$

where, the fitted values are $\mu_0 = 0.57$, $d_{c\mu} = 1.12$ μm and $d_{g\mu} = 1790$ μm with "c" denoting cohesion and "g" geometry. In Fig. C1, the curve $\mu 1$ represents the first contribution inversely proportional to d_{50} due to inter-particle cohesion, which decays to zero with increasing particle size and it has the same power law as the cohesive strength, see Fig. 19(b). In contrast, the second term $\mu 2$ is an empirical relation due to contributions from particle geometrical/inter-locking, which increases with particle size. The combination of these two contributions gives the total steady state bulk friction of the limestone powders in Eq. (1C).

Author's short biography

Hao Shi

Hao Shi is a PhD candidate in the MSM (Multi-Scale Mechanics) group at the faculty of engineering technology (ET) chaired by Prof. Stefan Luding at University of Twente, the Netherlands. He completed his BEng degree in refrigeration and air-conditioning engineering at Nanjing Institute of Technology (2011), China. He received his MSc degree in chemical and energy engineering at Otto-von-Guericke University (2013), Magdeburg, Germany, where he worked in the mechanical process engineering group chaired by Prof. Jürgen Tomas. Later, he joined the MSM group in 2014 for his PhD study which is based on the Marie Curie training network "T-MAPPP". His research interests range from tabletting processes for cohesive powders to discrete element simulations of granular assemblies with the development of calibration and validation protocols as well as other industry-relevant research studies. He collaborates with other researchers in various institutions and industries including TU Braunschweig in Germany, UT Compiegne in France, P&G in UK and the university of Edinburgh in UK.

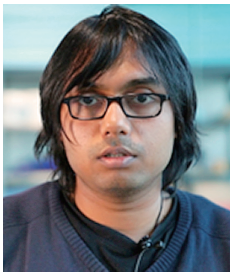

Rahul Mohanty

In 2013, Rahul Mohanty completed his master studies in Material Resource Engineering at AcSIR University, India. In the same year, he joined CSIR-IMMT, India, as a Quick Hire Scientist for a one-year internship. In September 2014, he joined iPAT—research group "Bulk Solids and Granular Matters" as a research associate in TU Braunschweig, Germany. Later in September 2015, he moved to P&G UK, Newcastle, continuing his research as a research scientist based on the Marie Curie training network "T-MAPPP". His research interest is to investigate the dry as well as wet contact adhesion for the chosen processes, in order to develop a DEM model for quasi-static and dynamic processes and validation against simple tests, and to develop an upscaling procedure from a DEM particle model to process a scale compartment model.

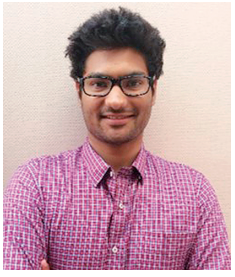

Somik Chakravarty

Somik Chakravarty completed his BEng in mechanical engineering at the University of Sheffield and MSc in Thermal power and fluids engineering at the University of Manchester, UK. He is presently on an EU FP7 Marie Curie fellowship (T-MAPPP) working as an early stage researcher at the University of Technology of Compiègne (UTC), France, in the field of characterization of mechanical properties of bulk solids. His research interests include powder handling and processing, characterization of powders by their flow properties and dustiness. He collaborates with researchers in academia and industry including TU Braunschweig, BASF, INERIS, and the University of Twente.

Author's short biography

Ramon Cabiscol Martinoli

Ramon Cabiscol studied chemical engineering from 2008 to 2013 at the Institut Químic de Sarrià in Barcelona. He received a DAAD scholarship in 2013 for postgraduate students to perform a research internship at the Technische Universität Braunschweig. His scientific interests include powder handling and flowability, tableting technology and numerical modelling of compaction. He is currently part of the Marie Curie training network "T-MAPPP". He is carrying out his PhD on "Modelling of abrasion of pharmaceutical tablets" at the Institute for Particle Technology and the Center for Pharmaceutical Engineering (PVZ), both in Braunschweig.

Martin Morgeneyer

Martin Morgeneyer works at Compiègne University of Technology (UTC), France, and his research focuses on powder and particle properties. He studied in Braunschweig, Compiègne and Zaragoza, received his degree in mechanics and his PhD in powder mechanics from the Technical University of Braunschweig, Schwedes' group. Prior to joining UTC as VP International Relations, Morgeneyer worked at Unilever in Warrington, and was responsible for internationalization at the Faculty of Mechanical Engineering at Braunschweig, of which he became the managing director later on. He now serves as chair of the Working Party on Characterization of Particulate Systems at the EFCE.

Harald Zetzener

Harald Zetzener studied mechanical engineering from 1989 to 1996 at the Technische Universität Braunschweig. He finished his PhD thesis on "Determination of rate-dependent deformation behaviour of cohesive powders in a bi-axial test" in 2002. He performed a post-doc at the Telemarks Technical Research and Development Centre in Porsgrunn, Norway. Afterwards he worked as Supply Quality Manager for Reckitt Beckinser before assuming the position of Deputy Director of the Institute for Particle Technology. His field of expertise is particle technology and design of equipment.

Jin Ooi

With a BEng (Hons) degree from the University of Auckland and a PhD from the University of Sydney, Jin Ooi joined the University of Edinburgh in 1990 and has been the professor of Particulate Solid Mechanics since 2005. His research covers both computational and experimental studies of of powders and solids, from particle phenomena to bulk characteristics, and applications in industrial processes. Jin enjoys collaboration with academic and industrial partners. He has published extensively with over 150 journal and conference papers and several book chapters. He is on the editorial board for Canadian Geotechnical Journal and Acta Geotechnica, and has co-founded DEM Solutions Ltd. and Particle Analytics Ltd.

Author's short biography

Arno Kwade

Arno Kwade studied mechanical engineering from 1986 to 1992 at the Technische Universität Braunschweig and the University of Waterloo. He finished his PhD thesis on "Autogenous Grinding in Stirrred Media Mills" in 1996. Afterwards he worked as general manager and executive director before he started his career as full professor for mechanical process engineering in 2005 at the Institute for Particle Technology. He is the head of the Centre of Pharmaceutical Engineering (PVZ) and member of the board of the Automotive Research Centre Niedersachsen (NFF). His main research focuses on experimental and numerical investigations in the fields of grinding and dispersing, flow and compression of powders as well as preparation of particulate coatings.

Stefan Luding

Stefan Luding studied physics at the University of Bayreuth, Germany, on reactions on complex and fractal geometries. He continued his research and moved to Freiburg for his PhD on simulations of dry granular materials in the group of polymer physics with-Prof. A. Blumen. Then he spent his postdoc time in Paris VI, Jussieu, with E. Clément and J. Duran before he joined the group of Computational Physics with Prof. Herrmann, where he did his habilitation. In 2001, he moved to DelftChemTech at the TU Delft in Netherlands as Associate Professor in Particle Technology. Since 2007 he holds the chair on Multi-Scale Mechanics (MSM) at the Faculty of Engineering Technology, ET, at the University of Twente, the Netherlands, with ongoing research on fluids and solids, particles and their contacts, granular materials and powders, asphalt, composites, bio- and micro-fluid systems and self-healing materials. Since 1998 he is managing Editor in Chief of the journal Granular Matter and since 2005 president of AEMMG, the scientific organizing committee of the Powders & Grains conference series.

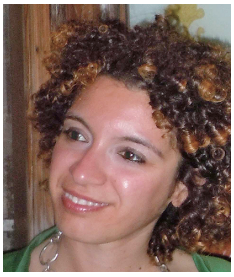

Vanessa Magnanimo

Vanessa Magnanimo is an Assistant Professor (UD1) in the Department of Thermal and Fluid Engineering within the Faculty of Engineering Technology at the University of Twente. She is part of the Multi-Scale Mechanics group. Vanessa received her MSc degree in construction engineering from the Politecnico of Bari, Italy, and received her PhD in Continuum Mechanics from the same university. After her PhD and before joining the University of Twente as a postdoc in 2010, she worked as a consultant in a structural engineering firm. She was a visiting scientist at the Levich Institute—CCNY and at T&AM—Cornell University. Vanessa is currently principal investigator in EU- and industrially-funded projects. She was part of the editorial board for Géotechnique and Powder Technology and is presently chair of the Female Faculty Network Twente. Vanessa's broad research interests are primarily in the area of theoretical analysis and modern simulation techniques applied to constitutive modelling of materials with an internal micro-structure such as soils and powders.